

INVESTIGATION AND DEVELOPMENT OF PASSIVE DAYTIME RADIATIVE COOLING DEVICES



A Thesis

by

PAUL MCKINLEY

Submitted to the Department of Physics & Astronomy
Pomona College
in partial fulfillment of the requirements for the degree of
BACHELOR OF ARTS

May 2022

Author: Paul McKinley

Advisor: Dr. Janice Hudgings

May 5, 2022

Table of Contents

ABSTRACT	ii
ACKNOWLEDGMENTS	iii
1. INTRODUCTION AND LITERATURE REVIEW	1
1.1 A Growing Need for Cooling.....	1
1.1.1 The Carnot Efficiency Limit and Cold Reservoirs	1
1.1.2 Atmospheric Transparency Windows	2
1.2 Criteria for Passive Daytime Radiative Cooling (PDRC)	3
1.3 Approaches to Passive Cooling.....	4
1.3.1 Layered Materials	5
1.3.2 Refractive Material Combinations	6
1.4 Applications & Implementation	7
1.4.1 Applications	7
1.4.2 Implementation	8
1.5 Summary	8
2. THEORY OF PASSIVE RADIATIVE COOLING	9
2.1 Blackbody Radiation and Spectral Properties	9
2.2 Radiative Exchange on Earth's Surface	12
2.3 Mechanism of Passive Cooling	16
2.4 Summary	18

3. EXPERIMENTAL METHODS	19
3.1 Fabricating Passive Cooling Thermal Emitters	19
3.1.1 Preparation of Wafer Substrates: Silicon and Fused Silica.....	22
3.2 Developing an Experimental Set-Up	25
3.2.1 Constructing a Housing Apparatus with Minimal Parasitic Effects.....	25
3.2.2 Outdoor Experiment.....	28
3.3 Summary	30
4. RESULTS AND DISCUSSION	31
4.1 Rooftop Experiment Results.....	31
4.1.1 Experiment 1: Silicon Devices.....	32
4.1.2 Experiment 2: Fused Silica Devices.....	36
4.1.3 Experiment 3: Adapted Silicon Devices	38
4.1.4 Discussion	41
4.2 Progression of Experiments	43
4.2.1 Initial Testing	43
4.2.2 Experimental Set-Up Modifications	45
4.3 Device Construction	48
4.4 Summary	49
5. CONCLUSION AND FUTURE DIRECTIONS	50
5.1 Future Directions	51
5.1.1 Experimental Set-Up	51
5.1.2 Spectral Analysis	53
5.1.3 Theory and Calculations	53
5.1.4 Novel Device Structures	54
5.2 Concluding Remarks.....	54

REFERENCES	56
APPENDIX A. DEVICE FABRICATION PROCESS.....	59
A.1 Wafer Preparation and Cleaning.....	59
A.2 Using the Thermal Evaporator.....	60
A.2.1 General Notes.....	60
A.2.2 Specific for PDRC Silver Deposition.....	60
A.3 Application of Polydimethylsiloxane	61
A.3.1 Mixing PDMS	61
A.3.2 Blade Coating Procedure.....	61
A.3.3 Spin-Coating Method	62
APPENDIX B. TEMPERATURE LOGGING TESTING APPARATUS	64
B.1 General Notes on Experimental Set-Up.....	64
B.2 Arduino Code	64

ABSTRACT

This thesis presents preliminary proof-of-concept research into developing passive daytime radiative cooling devices. Passive radiative cooling enables surfaces to cool to below-ambient temperatures by emitting thermal radiation selectively in the infrared while minimizing absorption over all other wavelengths. As the first project to focus on passive cooling research at Pomona College, our work outlines the context and theory behind passive radiative cooling, which has important applications in building materials, rooftop coatings, electronic devices, and interior air conditioning. We outline our design and fabrication process for two types of passive cooling devices built on silicon and fused silica substrates based on results from the literature, as well as the construction of a testing apparatus to record the device temperatures in an outdoor rooftop environment. Our devices cool to temperatures that average 3 - 3.5 °C below ambient surroundings, and nearly 20 °C below our silicon experimental control while under direct sunlight. This margin of cooling could be especially important in preventing overheating from continuous solar exposure, and serves as a promising benchmark for continued research in this area.

ACKNOWLEDGMENTS

I would like to express my thanks to so many members of the Pomona Physics and Astronomy community, who were not only helpful in the development of this thesis, but have also been tremendously supportive and encouraging during my time at Pomona College. Thank you to Haidee and Kylie for their helpful feedback and discussion in senior seminar. I am proud to be a member of the "Team Green" thesis reading group. I would also like to thank Professor Mawhorter for his support and feedback in both senior seminar and advanced laboratory when I first began investigating passive radiative cooling. I am very appreciative to Profe Moreno for reading and providing feedback on this thesis. Thank you to Hardy, whose help in designing and constructing my experimental apparatus was absolutely invaluable. I am additionally so grateful to Tony, whose assistance with my circuit design and temperature logging set-up were instrumental in turning a list of ideas in a lab notebook into an experiment. I would also like to thank Dave Haley, Professor Taylor, and Joseph Beardslee for their advice, discussion, and seemingly endless supply of creative solutions to my research quandaries, as well as Gordy for helping talk through different experimental methods as I was just starting this project. I am so appreciative of all the members of the Hudgings lab who helped show me the ropes of the chem prep lab and whose enthusiasm and commitment to their work is a constant and welcome motivator. Thank you also to Genevieve for her assistance, suggestions and patience in the multiple stages of the experimental design and testing processes. Finally, thank you so much to Professor Hudgings for her continued support and encouragement throughout every step of this thesis. I could not ask for a better advisor for a brand new project that brought with it excitement and challenges. Her guidance, mentorship, and commitment to her students has continually inspired me, as I know it has so many others in the Pomona College community. Thank you, all.

1. INTRODUCTION AND LITERATURE REVIEW

1.1 A Growing Need for Cooling

Cooling processes are vital for many aspects of society, including housing, electronic devices, transportation, food production and storage, and global supply chains. However, current methods of cooling are extremely energy-intensive. Cooling processes currently account for approximately 17% of electricity demand globally, and interior air conditioning alone accounts for approximately 15% of electricity consumption in U.S. buildings, and as much as 70% of consumption in humid equatorial regions [1][2]. Furthermore, energy demand for cooling is projected to increase by 72% by the year 2100, due to population increases, urbanization, and warming due to global climate change [3]. In addition to the environmental impact of heavy electricity demand, the cooling sector additionally accounts for more than 10% of global greenhouse gas emissions[1]. Most compression-based cooling systems release high amounts of carbon dioxide and hydrofluorocarbons while also relying heavily on the use of other pollutants such as ozone [1][4]. Furthermore, standard air conditioning methods simply displace warm air, typically cooling an interior by dispersing heat to the ambient surroundings. Conventional methods of air conditioning are therefore not only energy-intensive and costly, they actively contribute to the greenhouse effect and net global warming. Passive radiative cooling is an electricity-free method of reducing the temperature of surfaces by combining materials that exhibit specific optical and radiative properties over the ultraviolet, visible, and infrared regions of the electromagnetic spectrum. This project seeks to expand on a growing body of research developing passive cooling devices that are cost-effective, pollutant-free, and require no external power supply after production.

1.1.1 The Carnot Efficiency Limit and Cold Reservoirs

The need for electricity-free methods of cooling can be illustrated using the Carnot efficiency limit as a model. Although the Carnot limit describes the maximum theoretical, and thus impractical, efficiency of a heat engine, it is helpful in modeling many energy conversion processes. Under

the Carnot engine model, spontaneous heat flow between a hot and cold reservoir is converted into useful work. The maximum efficiency of this "engine" can be obtained from the temperatures of the hot and cold reservoirs, expressed as

$$\eta = 1 - \sqrt{T_C/T_H}, \quad (1.1)$$

where η is the efficiency expressed as a fraction, T_C is the temperature of the cold reservoir, and T_H is the temperature of the hot reservoir. With a surface temperature of approximately 6,000 K, the sun is an important "hot reservoir" for many energy conversion processes, including renewable energy sources such as solar photovoltaics. Similarly, renewable and nonrenewable methods of energy conversion rely on the surrounding air in Earth's atmosphere, at a temperature of approximately 250 K, to be a cold reservoir. However, under the influences of anthropogenic climate change, we are witnessing increasing surface and near-surface air temperatures. This means that from our Carnot model, the value of T_C is rising on a global scale, suggesting that a warmer atmosphere near Earth's surface reduces the efficiency of many energy conversion processes [5].

In order to limit this steady reduction of efficiency, a more reliable cold reservoir is desired. Whereas the average near-surface atmospheric temperature is around 250 K (approximately 50 K below room temperature), the average temperature of outer space is around 3 K, making it the coldest known reservoir to which we have access [4]. Thus, by using outer space as a cold reservoir, we can both increase the efficiency of energy-conversion and cooling processes while decreasing contributions to surface warming.

1.1.2 Atmospheric Transparency Windows

Most terrestrial entities emit blackbody radiation over broad ranges of the infrared (IR) portion of the electromagnetic spectrum. Significant portions of this upward IR radiation are absorbed by atmospheric gases, thereby retaining heat in the atmosphere and giving rise to the greenhouse effect. However, narrow regions exist over the IR wavelengths that are not subject to atmospheric absorption, allowing upward thermal radiation to escape directly to the cold of outer space. These

wavelength regions over which heat is not absorbed by the atmosphere are termed "atmospheric transparency windows" [4][6].

The primary atmospheric windows exist between 8-13 μm and, to a lesser extent between 16-22 μm (See Figure 1.1). The 8-13 μm window is most effective at allowing IR radiation to pass through the atmosphere to space, and additionally coincides with the peak emissivity of many terrestrial surfaces [4]. While high emittance over these wavelengths allows such surfaces to cool off at night, the cooling effect is supplanted by solar heating during the daytime [7]. Therefore, in order for continuous passive cooling to occur, structures must both maximize thermal emittance in the atmospheric transparency window while also reducing the solar absorption during the daytime.

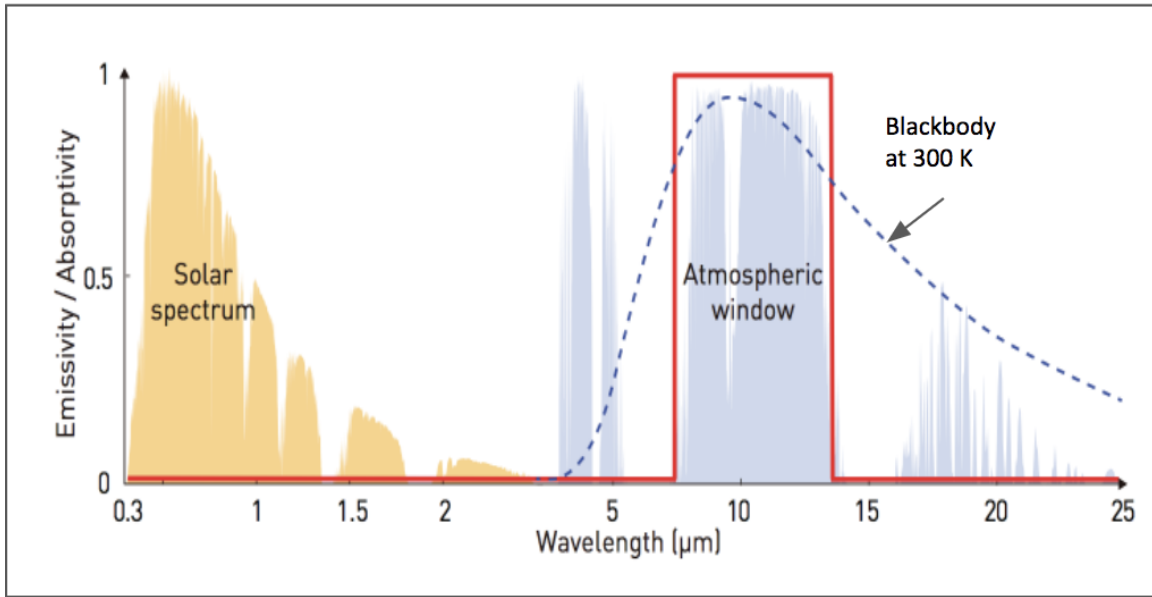


Figure 1.1: Emissivity (and equivalently absorptivity) plotted vs. wavelength for an ideal passive cooler (red line). For reference, a normalized solar spectrum (orange), the atmospheric transparency window (blue), and a normalized radiation spectrum at 300 K (dashed line). Adapted from [8].

1.2 Criteria for Passive Daytime Radiative Cooling (PDRC)

Passive radiative cooling refers to an object's intrinsic tendency to emit more energy than it absorbs without any external energy input. This method of cooling can be traced back to ancient

Iranian courtyards designed to passively cool at night, and most passive cooling research in the 20th century has focused almost exclusively on nighttime passive cooling [9][10]. Recent work, however has focused on implementing passive cooling during the *daytime*, when it is needed most [6][7][11][12]. Achieving passive daytime radiative cooling (PDRC) requires surfaces to exhibit specific spectral properties over different wavelength ranges that counteract warming from the sun. Yang et al. outline three criteria needed for a surface, commonly known as a thermal emitter, to achieve PDRC [4]. First, thermal emitters must be nearly 100% reflective ($R = 1$) over solar wavelengths, conventionally defined as 0.15-4 μm . This is intended to limit heating from solar radiation. For materials with zero transmittance ($T = 0$), the material's reflectivity is related to its absorptivity by $R = 1 - \alpha$, where α is the object's thermal absorptivity. This necessitates $\alpha = 0$, meaning no solar absorption occurs. Second, the surface must have a high emissivity ($\epsilon = 1$) over the wavelengths corresponding to the atmospheric transparency window (8-13 μm). This means maximizing outgoing radiation over wavelengths that will not be absorbed by atmospheric gases. By Kirchoff's law of thermal radiation, absorptivity corresponds to emissivity ($\alpha = \epsilon$),¹ thereby implying that we must also have high absorptivity and thus low reflectivity over the atmospheric window wavelengths ($\alpha = \epsilon = 1, R = 0$). Finally, a thermal emitter should have as high of reflectivity as possible over all other infrared wavelengths ($R = 1, \alpha = \epsilon = 0$). While this condition is not as critical, it is important for achieving surface cooling below ambient temperatures, since high reflectivity over all wavelengths outside of the atmospheric window limits the potential for radiative heating from the atmosphere [4]. This effect is illustrated in Figure 1.2. The details of reflectivity, absorptivity, and emissivity are discussed further in Chapter 2.

1.3 Approaches to Passive Cooling

An extensive suite of methods and materials have been tested in the literature in order to achieve consistent PDRC to sub-ambient temperatures [9]. Most approaches fall into one of two categories: (1) layering planar materials together with different optical and radiative properties, and

¹Kirchoff's law of thermal radiation applies only when an object is in thermal equilibrium with its environment. This condition is assumed for the theory presented.

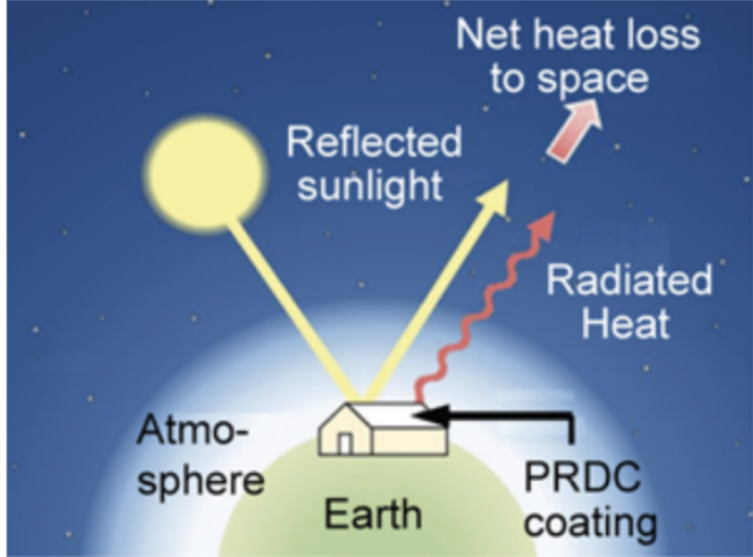


Figure 1.2: A schematic of the general goal of passive daytime radiative cooling in a rooftop application. Adapted from [4].

(2) mixing materials that each have different refractive indices, leading to high reflectance over solar wavelengths [4]. Our experimental approach falls mostly into approach (1), using low-cost, polymer-based materials. However, we also note some of the promising techniques in both categories, as the efficacy of PDRC emitters varies widely based on both the geographic region and specific application in which they are implemented.

1.3.1 Layered Materials

Since a passive cooling thermal emitter should have high reflectance over solar wavelengths and high emittance over long-wave infrared (LWIR) wavelengths, specifically those in the atmospheric transparency window, one strategy for passive cooling is to simply combine materials that individually exhibit these desired properties. Such an approach typically involves layering an IR-emissive coating over a highly reflective substrate, such as aluminum (Al) or silver (Ag), as shown in Figure 1.3. This approach enables a higher degree of spectral tuning by combining materials with different emittance and reflectance over the electromagnetic spectrum. For example, Raman et al. demonstrated daytime cooling under direct sunlight of 4.9 °C below ambient temperatures by constructing an emissive coating of seven alternating layers of silicon dioxide (SiO_2) and hafnium

dioxide (HfO_2) on a silver-coated silicon substrate [6]. Kou et al. employed a similar approach by applying an emissive coating of the commercially-available polymer, polydimethylsiloxane (PDMS) to a silver-coated fused silica substrate, achieving sub-ambient temperature reductions of 8.2°C under direct sunlight and 8.4°C at night [12].

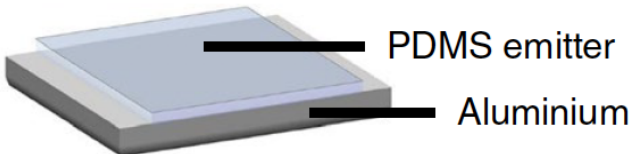


Figure 1.3: A simple depiction of the layered material approach to passive cooling, with an emissive polymer layered over aluminum which serves as good solar reflector [7].

1.3.2 Refractive Material Combinations

Another approach to PDRC design involves combining materials with different refractive indices that leads to optical scattering and a high solar reflectance within the device [4]. If two materials with different refractive indices are largely transparent over the same wavelength range, the optical scattering at the material interface can minimize light absorption. Yang et al. describe the example of snow, which is comprised of ice crystals and air pockets, each of which has a different index of refraction ($n = 1.31$ and $n = 1$, respectively). Scattering at the interface results in an overall solar reflectance of 90% [4]. Methods in the literature take a similar approach of strategically utilizing the refractive index of air by increasing the porosity of a reflective material that also has substantial LWIR emissivity. For example, Mandal et al. created a porous coating of poly(vinylidene fluoride-co-hexafluoropropene) [$\text{P(VdF-HFP)}_H\text{P}$] that could be deployed on rooftops and was more reflective over solar wavelengths than existing "cool roof paints," achieving a maximum sub-ambient cooling of 6°C [13]. This process has also been recently explored in organic materials. Lin et al. processed wood through delignification and compression, finding that the stretching and rearrangement of cellulose fibers allowed for high optical scattering and

reflectance over solar wavelengths, as well as higher emissivity over LWIR wavelengths. Their structures achieved sub-ambient cooling of $>4^{\circ}\text{C}$ during the day and $>9^{\circ}\text{C}$ at night [14]. While our project does not explore the method of strategic optical scattering, it is worth mentioning both as a promising avenue for PDRC research, and because it may have benefits in scalability and application.

1.4 Applications & Implementation

1.4.1 Applications

As demand for cooling increases, there is no shortage of applications for electricity-free methods of heat dissipation. Applications that require a relatively large surface area and require constant cooling would benefit from applying a passive cooling thermal emitter to be directly in contact with the surface intended to be cooled. For example, a planar passive cooler such as that described in subsection 1.3.1 could be implemented as a cover for rooftop materials. This would be particularly useful in regions at risk of extreme heat and the urban heat island effect [15][16]. A similar approach could be used in materials for temperature-sensitive shipping containers and even vehicles that expend high amounts of energy for air conditioning [4]. Some work has also been done to investigate the potential for passive cooling in solar photovoltaic (PV) systems that could increase efficiency and prevent thermal degradation [17].

The direct contact approach can work on large spatial scales, but lacks the benefit of on-demand cooling. Goldstein et al. showed how passive cooling can be used to modify fluid temperatures that can then modulate interior building temperatures [2]. Although more prone to parasitic heat loss, this represents a higher degree of temperature control than a direct contact thermal emitter. In addition to temperature modulation, passive cooling has also been explored as a means of off-grid energy production when coupled with a thermoelectric generator, although the current power generated from this method (0.5 W/m^2) is not yet scalable [18].

1.4.2 Implementation

Cost, scalability and environmental conditions all pose challenges to implementing passive radiative coolers in practical settings. One of the motivations for this project is to experiment with low-cost, commercially-available materials. Although high rates of cooling have been demonstrated using more complicated materials, such as laboratory-fabricated dielectric stacks and nanoparticle-based solutions, it is important to refine and optimize approaches that can be manufactured on large scales with a short payback time.

Environmental conditions also serve as a major challenge for passive cooling implementation. Humidity and cloud cover, in particular, have been implicated as significant inhibitors of outgoing radiation through the atmospheric window [19]. While experimenting with different outdoor environmental conditions is beyond the scope of this project, it is worth noting that some research groups have been working to identify materials that can maximize cooling in high-humidity environments [11]. An important consideration in the field of PDRC is that the optimal cooling solutions, both in material structure and sector of application, will be heavily influenced by regional climates and environmental conditions.

1.5 Summary

Passive cooling is an electricity-free method of heat dissipation that does not contribute to the greenhouse effect and can potentially lead to below-ambient surface temperatures, even under direct sunlight. This chapter is intended to introduce the field of passive radiative cooling and its fundamental physical principles, highlighting notable examples from the literature and potential applications. The following chapters outline an exploratory project to test the feasibility of developing passive daytime radiative cooling devices at Pomona College, using low-cost, commercially-available materials.

2. THEORY OF PASSIVE RADIATIVE COOLING

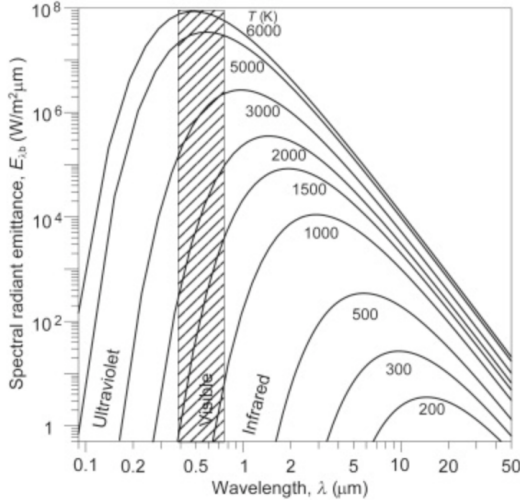
Passive radiative cooling is fundamentally characterized by energy exchanges between a reflecting and radiating surface and the cold of outer space. Constructing a successful radiative cooler necessitates an understanding of the spectral properties of the cooler device, in particular its tendency to absorb or reflect solar radiation, in addition to infrared radiation from the atmosphere. The theory behind this process is divided into three fundamental pillars in this chapter: (1) governing properties of blackbody and near-blackbody emitters at Earth's surface, (2) atmospheric dynamics that lead to both the greenhouse effect and transparency windows, and (3) the energy exchanges that relate the two.

2.1 Blackbody Radiation and Spectral Properties

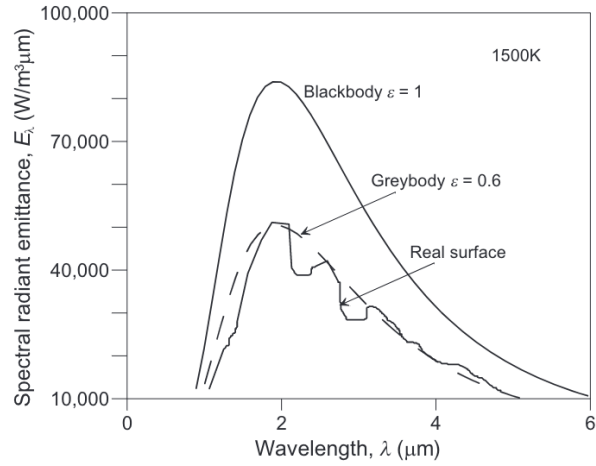
An object with a finite temperature will radiate energy to its surroundings in the form of discrete quanta of energy known as photons [9]. The distribution of this radiated energy over wavelengths in the electromagnetic spectrum depends on both the material composition of the object, as well as its temperature [20]. An ideal "blackbody" emitter is a theoretical object that absorbs and re-emits all incident radiation and corresponds to the maximum thermal radiation emanating from an object at a given temperature. This absorbed and emitted radiation is denoted as a blackbody's spectral irradiance per unit area per wavelength and can be expressed using Planck's law of blackbody radiation:

$$I_{BB}(T, \lambda) = \frac{2hc^2}{\lambda^5} \frac{1}{e^{hc/(\lambda k_B T)} - 1}, \quad (2.1)$$

where h is Planck's constant ($h = 6.63 \times 10^{-34}$ J·s), k_B is the Boltzmann constant ($k_B = 1.38 \times 10^{-23}$ J·K $^{-1}$), T is the object's temperature in Kelvin, λ is the wavelength of electromagnetic radiation in meters, and c is the speed of light ($c = 2.99 \times 10^8$ m/s) [6][9]. This irradiance, also known as the power density, is both temperature and wavelength-dependent, while all other terms in the expression are constants. The conventional units of I_{BB} are therefore W/m 2 if we define



(a) Blackbody curves for temperatures from 200K-6000K, calculated using Equation 2.1



(b) Comparison of blackbody, greybody, and realistic surface emittance spectra.

Figure 2.1: Blackbody spectral comparisons for varied temperatures and emissivities. Adapted from [20].

our wavelength of light in meters. We can obtain the total power emitted from a blackbody by integrating the irradiance in Planck's law over all wavelengths, for a given temperature, T . This radiated power is given by the Stefan-Boltzmann law:

$$P = \sigma T^4, \quad (2.2)$$

where T is the temperature of the object, P is the radiated power in W/m^2 and σ is the Stefan-Boltzmann constant ($\sigma = 5.67 \times 10^{-8} \text{ W}/\text{m}^2 \cdot \text{K}^4$). Figure 2.1a depicts several blackbody spectra at different temperatures, in which a larger area beneath the blackbody curve corresponds to a higher temperature and thus larger emitted power. Blackbody characteristics serve as an important reference in understanding radiative transfer, which comprises the basis of passive radiative cooling.

2.1.0.1 Reflectance, Transmittance, Absorptance, and Emittance

In reality, however, objects do not absorb and re-emit incident radiation as blackbodies. For a given surface, we assume that, while some fraction of incident light will be absorbed and re-emitted like a blackbody, another proportion may also be reflected off the object's surface or transmitted through the object entirely. Conservation of energy requires that these fractions of the total incident light add to one, given by

$$R + T + \alpha = 1, \quad (2.3)$$

where R is the reflectance, T is the transmittance, and α is absorptance.¹ Reflected and transmitted light will not change an object's temperature. Absorbed light, however, will cause an object's temperature to increase until it reaches thermal equilibrium [21].

What prevents the object from heating up indefinitely from absorbed light is the object's tendency to emit radiation. This is defined as the "emissivity" of an object, a spectral-dependent, dimensionless ratio that represents the fraction of blackbody radiation emanating from an object at a given wavelength and temperature, ranging from 0 to 1 [9]. Emissivity aggregated over all wavelengths therefore determines the "emittance" of the object, the total fraction of incident light lost as thermal radiation. The impact of emissivity on a blackbody curve can be seen in Figure 2.1b, in which an emissivity $\epsilon < 1$ of an object reduces the emitted power of the object. Emissivity plays an important role in passive cooling due to its wavelength dependence. A higher emissivity over wavelengths in the atmospheric window, for example, is a key criteria for sub-ambient passive cooling. In addition, the relationship between emissivity and absorptivity, the fraction of radiation *absorbed* by an object compared to a blackbody, is important for understanding radiative exchange between objects.

Kirchoff's law of thermal radiation states that an object's emissivity is equal to its absorptivity at a given wavelength ($\epsilon_{BB}(\lambda) = \alpha_{BB}(\lambda)$) when the object is in thermal equilibrium with its sur-

¹Some analyses of thin film spectra may also consider the potential for light to be diffusely scattered at the object's surface, in addition to being reflected, transmitted and absorbed. For the purposes of this theory, we do not consider diffuse scattering; however, taking direct spectral measurements of our samples in future work may wish to consider this term.

roundings [4][6][9]. A blackbody can serve as a motivating example, since we expect all incident radiation on the body to be completely absorbed and re-emitted. Since a blackbody, by definition, is at a constant temperature (in thermal equilibrium with its environment), the absorptivity and emissivity are equal

$$\epsilon_{BB} = \alpha_{BB} = 1. \quad (2.4)$$

Kirchoff's law additionally applies to non-blackbody emitters, so long as they are in thermal equilibrium with their surroundings. The interplay between spectral reflectance, transmittance, absorptance, and emittance underscores the basis of not only passive cooling, but radiative exchange between objects with non-zero temperatures in general. In this work, we use these spectral properties to relate energy transfer between the sun, Earth's atmosphere, and the surface of a thermal emitter to temperature variation in the emitter itself.

2.2 Radiative Exchange on Earth's Surface

2.2.0.1 Extending the Blackbody Model

Temperatures of ambient air and objects near Earth's surface are heavily impacted by the balance between radiation from the sun, atmosphere, and the planet's surface. To first order, the surfaces of the sun and Earth can be modeled as blackbodies [20]. The solar spectrum spans wavelength ranges from 0.15 μm to 4 μm , with peak irradiance centered at approximately 0.5 μm , corresponding to an average surface temperature of the sun of approximately 6000 K (Figure 2.2, left). In the absence of an atmosphere, the portion of Earth's surface facing the sun absorbs this radiation, which is mostly in the visible, ultraviolet, and near-IR portion of the electromagnetic spectrum, and re-emits radiation in all directions, primarily over mid-infrared wavelengths (Figure 2.2, right). The blackbody model of Earth peaks in this mid-IR wavelength region, reaching an equilibrium surface temperature of 255 K (-18 °C). This is significantly colder than the true average temperature of Earth's surface (around 288 K); however, the blackbody estimate is useful in providing a conceptualization of the distribution of radiation for the sun and Earth in isolation [20]. The planet's atmosphere and its surface-warming effects, commonly referred to as the "greenhouse

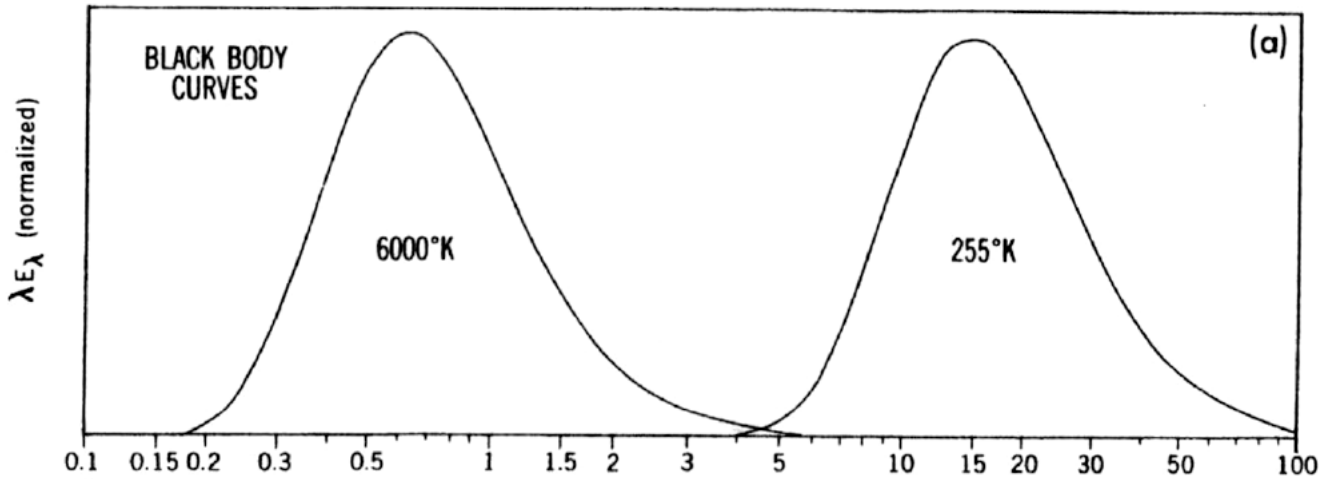


Figure 2.2: Normalized blackbody estimates for the sun and Earth against wavelength in micrometers. Adapted from [22].

effect," are the primary factors in this surface temperature correction.

2.2.0.2 Atmospheric Dynamics and Warming

The Earth's atmosphere is made up of approximately 78% nitrogen (N_2), 21% oxygen (O_2), and 0.9% argon (Ar), with the remaining 0.1% attributed to other trace gases [22]. Although the atmosphere is responsible for a portion of solar irradiation being reflected, including off the tops of clouds, the primary atmospheric gases themselves are largely transparent to sunlight. It is the thermal radiation in the infrared from Earth's surface, here termed "surface radiation," that is prone to atmospheric absorption. Nitrogen and oxygen are largely transparent to surface radiation, but many of the trace gases are not. Specifically, water vapor (H_2O), nitrous oxide (N_2O), ozone (O_3), and carbon dioxide (CO_2) are strongly absorptive of infrared radiation, and therefore have the largest impact on radiative energy fluxes near Earth's surface. Much of this absorption is attributed to the fact that these gases consist of three atoms per molecule, which enables greater absorption of thermal radiation through vibrational modes [9][22]. These trace gases therefore contribute to the greenhouse effect by absorbing upwelling radiation from Earth's surface and re-emitting it in all directions, including back towards the surface, leading to net warming. Carbon dioxide and

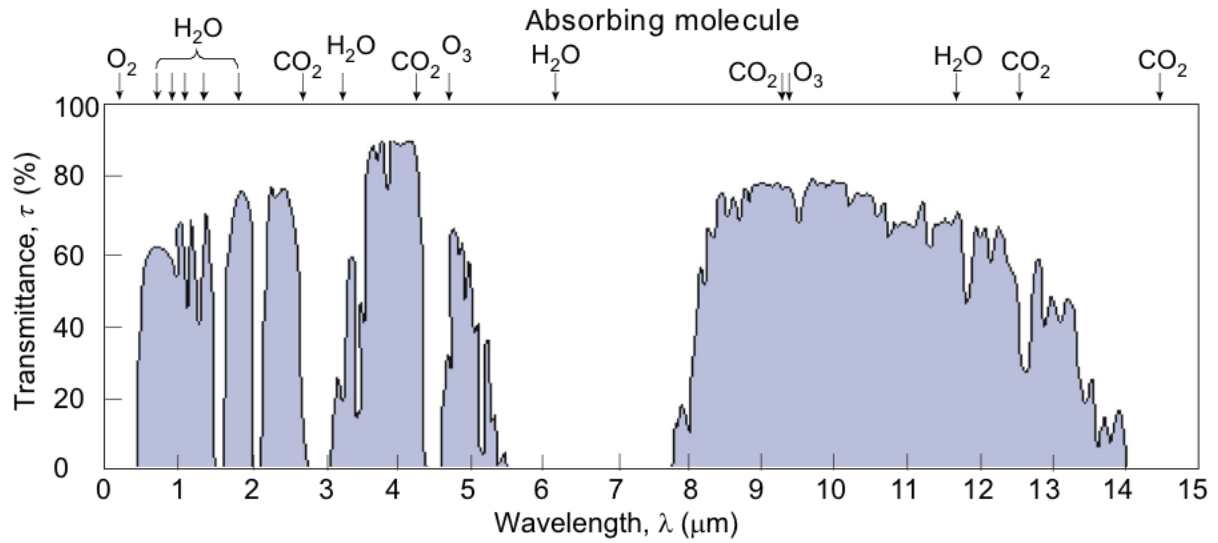


Figure 2.3: Transmittance of IR radiation and absorption lines for primary atmospheric trace gases. Figure does not account for fluctuation in relative humidity or variable pollutants. Adapted from [20].

water vapor play the most significant role in energy exchanges with Earth's surface, both because of their high concentrations in the lower-most atmospheric layer, the troposphere, and because of their specific absorption bands near the atmospheric transparency window [9][20][22].

Figure 2.3 shows atmospheric transmittance over mid-infrared wavelengths, and illustrates some of these absorption bands in the spectral "valleys." For example, we see that CO_2 has significant absorptions around $4.2 \mu\text{m}$ and $14.7 \mu\text{m}$. Water vapor similarly has a strong absorption band around $6-7 \mu\text{m}$, and although not depicted in Figure 2.3, is also a strong absorber of IR radiation beyond $20 \mu\text{m}$ [9][22]. The high degree of transmittance in the $8-13 \mu\text{m}$ range depicts the atmospheric transparency window. One of the key features of passive cooling is therefore to emit thermal radiation in wavelength regions with high atmospheric transmittance, away from the more substantial absorption bands in the mid-IR. Since passive cooling relies on maximizing transmitted heat through the atmosphere, these absorption bands are the primary inhibitors to maximizing cooling potential.

At the same time, there exist environmental challenges to selective thermal emission. The

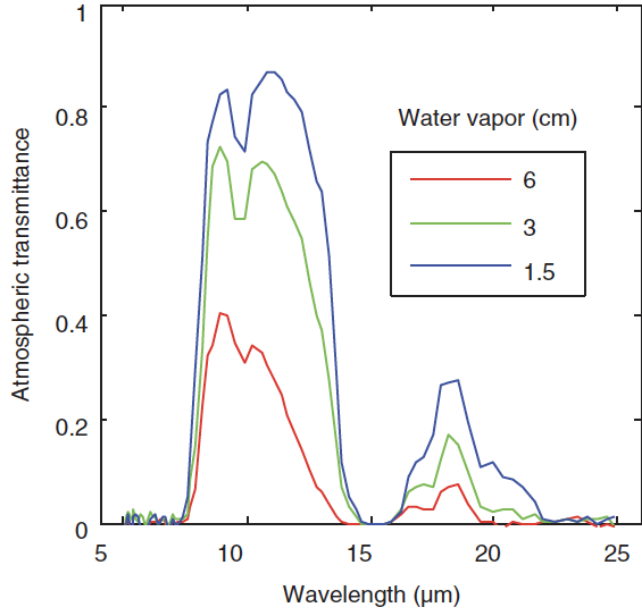


Figure 2.4: Atmospheric transmittance for varying levels of precipitable water vapor (cm). Higher relative humidity causes increased atmospheric absorption, thereby limiting the amount of radiation transmitted through the atmosphere. Adapted from [9].

precise absorptivity of water vapor, for example, is difficult to predict in wavelength regions near the atmospheric transparency window due to humidity [4][9]. Higher relative humidity in a region can cause higher absorption of radiant heat from water vapor in the 8-13 μm range, and thus limit the amount of energy transmitted through the atmosphere via passive cooling (Figure 2.4). Furthermore, the exchange of thermal radiation at Earth's surface is highly dependent on not only specific atmospheric constituents, but also their relative abundance, which can vary by geographic location, season, or short-term weather patterns.

Having explored the fundamental physics of radiating bodies, as well as the atmospheric conditions that overlay radiative exchanges between the earth and sun as radiating bodies themselves, we can now turn our attention to the resulting intersection that is passive cooling.

2.3 Mechanism of Passive Cooling

For a passive cooling surface at initial temperature T placed in ambient surroundings at T_{amb} , the total cooling power can be represented by the following energy balance equation²

$$P_{cool}(T) = P_{rad}(T) - P_{atm}(T_{amb}) - P_{Sun} - P_{cond+conv}, \quad (2.5)$$

where P_{cool} represents the net power flux of the surface as a function of the device surface temperature. $P_{rad}(T)$ represents the total outgoing radiation, also as a function of the device temperature. $P_{atm}(T_{amb})$ and P_{Sun} represent incoming radiation from the atmosphere at ambient temperature T_{amb} and the sun, respectively. $P_{cond+conv}$ similarly represents incoming power from any object with which the emitter is in contact (i.e. a rooftop) and air flow adjacent to the emitter.

Sub-ambient cooling occurs when the the net power flux, $P_{cool}(T)$ is positive, with the initial assumption that $T = T_{amb}$. Once the emitter reaches thermal equilibrium with its surroundings ($P_{cool}(T) = 0$) at temperature T_{eq} , passive cooling is evident when $T_{eq} < T_{amb}$.

The terms on the right hand side of Equation 2.5 can be characterized by incorporating the spectral and angular emissivity of the cooler, $\epsilon(\lambda, \theta)$. For a cooler with surface area A , our outgoing power is defined as

$$P_{rad}(T) = A \int \cos \theta d\Omega \int_0^\infty I_{BB}(T, \lambda) \epsilon(\lambda, \theta) d\lambda, \quad (2.6)$$

where the integral

$$\int d\Omega = 2\pi \int_0^{\frac{\pi}{2}} \sin \theta d\theta \quad (2.7)$$

refers to the angular integral over the hemisphere, and $I_{BB}(T, \lambda)$ describes the blackbody irradiance of the surface at a given temperature described in Equation 2.5. Additionally, in Equation 2.6, we have scaled the blackbody irradiance by the wavelength and temperature-dependent emissivity,

²The presentation for passive cooling theory in this chapter is adapted from derivations in the literature, from the following papers: [6][7][9][12]

$\epsilon(\lambda, \theta)$ and integrated over all wavelengths and angles in a hemisphere to derive an equation for total upward radiated power from our surface.

We can similarly express the radiated power from the atmosphere, absorbed by the cooler, as

$$\begin{aligned} P_{atm}(T_{amb}) &= A \int \cos \theta d\Omega \int_0^\infty I_{BB}(T_{amb}, \lambda) \epsilon_{atm}(\lambda, \theta) \alpha(\lambda, \theta) d\lambda \\ &= A \int \cos \theta d\Omega \int_0^\infty I_{BB}(T_{amb}, \lambda) \epsilon_{atm}(\lambda, \theta) \epsilon(\lambda, \theta) d\lambda, \end{aligned} \quad (2.8)$$

where we have similarly integrated the emitted energy from the surrounding atmosphere over all wavelengths and an angular hemisphere. However, we have additionally scaled this emitted energy by the absorptivity of the device, $\alpha(\lambda, \theta)$, to determine the thermal radiation that is absorbed by the surface. Finally, we substitute emissivity $\epsilon(\lambda, \theta)$ of the surface for absorptivity based on Kirchhoff's law. One way to conceptualize the atmospheric influence in passive cooling is to recognize that the $\epsilon_{atm}(\lambda, \theta)$ term in $P_{atm}(T_{amb})$ is naturally smaller for atmospheric window wavelengths since lower absorption is associated with lower emittance. For that reason, it is important to build passive coolers that maximize $\epsilon(\lambda, \theta)$ in the $P_{rad}(T)$ term to maximize outgoing radiation in this wavelength region.

The incident power absorbed by the surface due to sunlight can be represented as

$$P_{Sun} = A \int_0^\infty \epsilon(\lambda, \theta_{Sun}) I_{AM1.5}(\lambda) d\lambda, \quad (2.9)$$

where the θ_{Sun} is a fixed incident angle and $I_{AM1.5}$ is the intensity of an AM1.5 standard solar spectrum.³ Here, we let $\epsilon(\lambda, \theta_{Sun})$ represent the emissivity, and correspondingly the absorptivity, of the passive cooler over the solar spectrum. For the purposes of calculating radiative equilibrium at a given point in time, we take the sun to be at a fixed angle θ_{Sun} .

Finally, we assume some cooling power is reduced due to conductive and convective heating. This parasitic heat gain arises from radiative cooler being in contact with other objects (i.e.

³<https://www.pveducation.org/pvcdrom/appendices/standard-solar-spectra>

rooftops), as well as air flow adjacent to the cooler's surface. This is represented in the literature as

$$P_{cond+conv}(T, T_{amb}) = Ah_c(T_{amb} - T), \quad (2.10)$$

where h_c is a coefficient accounting for both convective and conductive heating.⁴ This section outlines the fundamental theory behind passive cooling from a radiative balance perspective. Equation 2.5 shows that a surface achieves net cooling when P_{cool} is positive, necessitating that P_{atm} , P_{Sun} and $P_{cond+conv}$ be minimized, while maximizing P_{rad} .

2.4 Summary

Daytime passive radiative cooling is comprised of a strategic combination of minimizing solar absorption while strongly emitting radiative heat in specific infrared wavelength regions at which transmission through the atmosphere is maximized. The discussion of passive cooling fundamentals in this chapter presents this interplay by first describing radiating surfaces as blackbodies, before exploring the nuanced relationship between reflectance, transmittance, absorptance and emittance, that arise from the limitations of the blackbody model. We additionally discuss radiative interactions between the sun, atmosphere, and objects near or at Earth's surface before finally detailing the power balance equations that govern temperature changes in passive cooling experiments.

⁴The expression for conductive and convective power may warrant additional consideration in modeling that uses these power balance equations. Calculations for the conductive power, in particular, should consider the temperature of the rooftop, as opposed to the ambient air temperature.

3. EXPERIMENTAL METHODS

Our work has two primary experimental components: (1) constructing low-cost passive daytime radiative cooling (PDRC) devices; and (2) testing the cooling potential of the devices in an outdoor setting. This chapter discusses the fabrication process for our passive cooling devices, also termed "thermal emitters," and the construction of our testing apparatus. We then outline the experimental design for testing our devices in an outdoor rooftop environment, as well as several pitfalls involved in initial testing.

3.1 Fabricating Passive Cooling Thermal Emitters

Our approach to passive cooling follows the method discussed in subsection 1.3.1, in which a reflective, planar surface is covered with a coating that is highly emissive in the 8-13 μm atmospheric window. In our devices, we apply a low-cost polymer, known as polydimethylsiloxane (PDMS), to a silver-coated wafer substrate. The layered wafer, or "thermal emitter" is housed in a sky-facing stand designed to minimize parasitic heating from conduction and convection in the surrounding environment. Although our focus in this project is to test the thermal emitters in outdoor rooftop environments, we also prepare samples that can be analyzed in a laboratory environment for direct spectral measurements.

Recent literature on experimental passive cooling has seen thin-film PDMS coatings as a promising feature in thermal emitter design. PDMS requires little preparation before deposition, and while it is largely transparent to sunlight, it is highly emissive in the mid-infrared atmospheric window [23]. Although individual preparations vary, we base the design of our emitters off of two particularly successful results from the literature. Zhou et al. prepare thermal emitters on aluminum substrates with a 150 μm coating of PDMS layered over top [7]. Aluminum serves as the reflective backing over solar wavelengths, while PDMS is the primary emissive layer. Figure 3.1 shows spectral measurements of the PDMS/aluminum thermal emitter, which achieves high emissivity in the atmospheric window and experiences relatively low absorption over the short-

wave infrared. One important finding from Zhou et al. is that variability in thickness and surface roughness of PDMS do not appear to affect overall emittance at a thickness higher than 100 μm . This experimental set-up achieves continuous cooling of 2-9 $^{\circ}\text{C}$ throughout daytime testing [7].

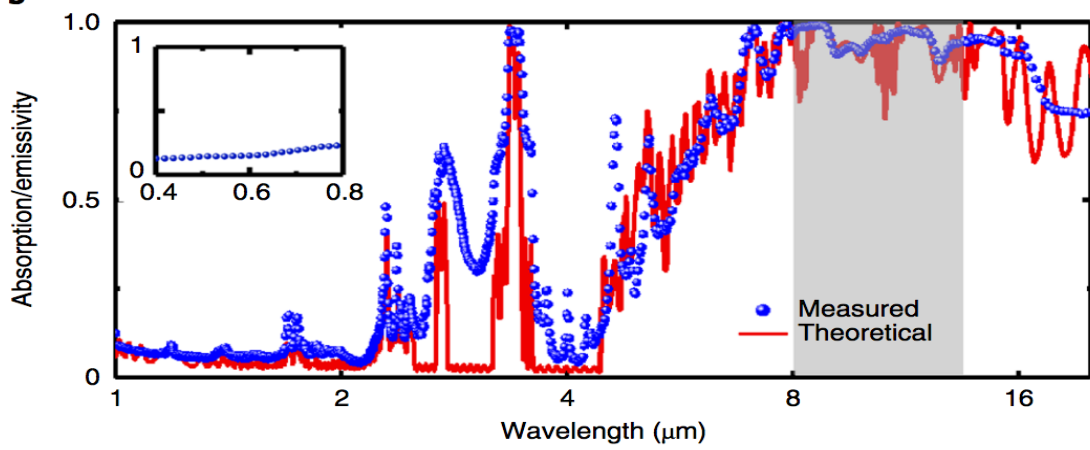


Figure 3.1: Theoretical and experimental spectral emissivity (equivalently absorptivity) of the PDMS/Aluminum passive cooler described in [7]. The gray band indicates the 8-13 μm atmospheric transparency window. The inset shows there is some absorption in the visible and near-infrared regions.

The second result is from Kou et al., in which a fused silica wafer is used as a substrate [12]. Fused silica is transparent in the visible and near-infrared portion of the electromagnetic spectrum, so to make the wafer reflective over solar wavelengths, a 120 nm coating of silver is deposited on the back of the wafer. PDMS is then coated on the top side of the wafer at a thickness of 100 μm . This differs from the set-up in Zhou et al., in that an additional reflective layer is deposited on the opposite side of the substrate relative to the PDMS. However, the general approach to couple an emissive polymer coating with a surface that is highly reflective over solar wavelengths remains constant. Similar to Figure 3.1, Figure 3.2 shows spectra for the thermal emitter used in Kou et al., as well as references for the solar spectrum, atmosphere, and several of the controls during testing. Of particular note is the comparison between the black line and red line in the 8-13 μm range. The black line tracks the emissivity of the complete thermal emitter with PDMS, which has a much

higher emittance in the atmospheric window than the red line, which represents a silver-coated silica wafer, with no PDMS layer. Results from Kou et al. and Zhou et al. thus suggest that PDMS is an important component of the passive cooling device construction for its emissive properties in the infrared.

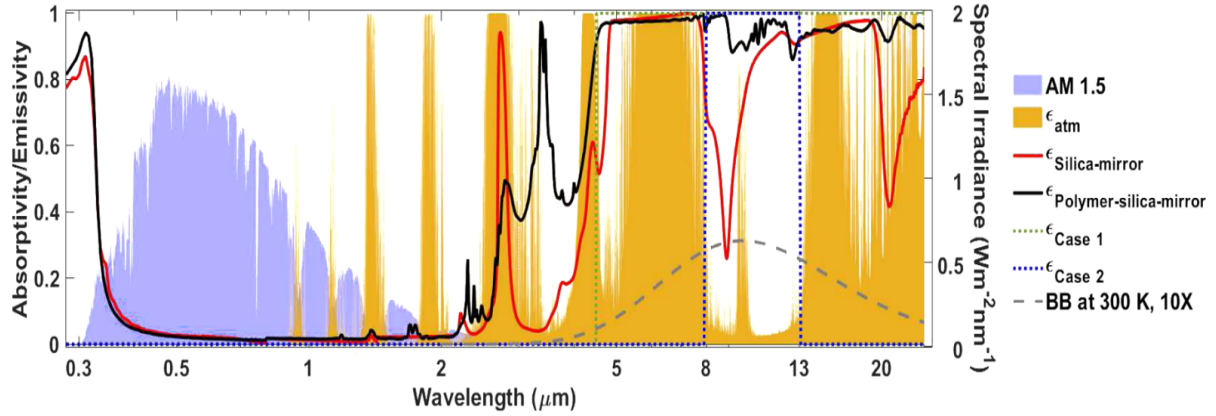


Figure 3.2: Spectral measurements of the PDMS/Ag/Silica passive cooler described in Kou et al. The black line shows the absorption (and hence emission) spectra of the complete passive cooler. Also pictured are the spectra of several experimental controls, the solar spectrum, the atmospheric absorption spectra, and a blackbody at 300 K. Adapted from [12]

In this work, we construct two sets of thermal emitters. The first design closely models that of Kou et al., with a fused silica substrate, and layers of silver and PDMS on opposite sides of the wafer [12]. The second design uses a silicon wafer as a substrate with stacked layers of silver and PDMS on top. This is closer to the set-up used by Zhou et al., in that the thermal emitter has PDMS layered over a reflective coating, but we use a different substrate and reflective material (silver layered over silicon instead of a single aluminum substrate) [7]. Fabricating these two types of emitters allows us to compare cooling potential with multiple substrates, as well as the layered designs in the literature.

3.1.1 Preparation of Wafer Substrates: Silicon and Fused Silica

Our silicon and fused silica wafers are both 500 μm thick and measure 100 mm in diameter, allowing us to directly compare the cooling potential in each type of emitter during testing. The identical dimensions also allow us to use the same cleaning and fabrication process for both sets.

3.1.1.1 Plasma Cleaning

Both the silicon and fused silica wafers used in this project are relatively new and in near-pristine condition, housed in dust-free containers. As a result, our process for cleaning each set of wafers is minimal. Each wafer is placed in a petri dish before being set in a Harrick Plasma PDC-001-HP plasma cleaner for three minutes. Plasma cleaning is done to remove organic contaminants from the surface of the wafer prior to any thin-film depositions. Specifications for plasma cleaning and the wafer fabrication process generally are discussed further in Appendix A.

3.1.1.2 Thermal Evaporation of Silver

Since neither substrate in our experiments is highly reflective over solar wavelengths, we deposit a layer of silver (Ag) onto the surface of each wafer. Immediately following the plasma cleaning process, we use an Angstrom Engineering NexDep System thermal evaporator to coat our wafers with 120 nm of silver under vacuum pressure. Although other reflective metals may be used, such as aluminum, we use silver in both of our set-ups for its high reflectance over solar wavelengths and high thermal conductivity [24]. Our initial thermal emitter prototypes consisted of square-inch wafers, allowing us to coat multiple wafers with silver at one time. Our larger, 100 mm diameter wafers must be coated one at a time, which lengthens the fabrication process. The silver layer maximizes the reflectance of the emitters over solar wavelengths, which precedes the application our emissive polymer coating.

3.1.1.3 Application of Polydimethylsiloxane (PDMS)

Polydimethylsiloxane (PDMS) is a low-cost, silicone organic polymer. PDMS is non-toxic and generally non-reactive, making it a popular material for use in a range of applications, such as soft

lithography, hydraulic fluids, caulking, and gel-based templates for electronic devices [25]. PDMS also has a relatively short curing time, making the deposition process relatively simple and fast. We make PDMS using a preset Sylgard 184 kit, mixing an elastomer base with a curing agent in a 10:1 base-to-curing agent ratio. The mixed PDMS is left covered under a fume hood for three hours to allow bubbles to naturally dissipate, which are not ideal for coating. The polymer is then manually blade-coated with a Teflon spatula over the prepared silicon wafer at a specified thickness.¹ The application of PDMS follows four steps:

1. **Application of a template:** The process of blade coating requires a template that can be laid over a substrate surface. When a polymer, or other non-solid coating is spread over the substrate, the template dictates the coating thickness. Here, we laser-cut a 98 mm-diameter circular hole into a compressed stock paper sheet, with a thickness of 0.50 mm (500 μm). Although this is a slightly smaller diameter than our wafer, the dimensions ensure that the paper template sits completely over the wafer (Figure 3.3a). After laying the paper template over the wafer, we set an identically-cut wax paper sheet over the template. The wax paper minimizes PDMS sticking to the paper template so that it may be re-used.
2. **Application of PDMS:** After the PDMS bubbles have dissipated, a small amount of the PDMS is poured onto an edge of the wafer that is not covered by the circular template. The PDMS should coat the entire edge of the wafer, within the border of the overlaid template (Figure 3.3b).
3. **Coating:** A Teflon spatula is used for coating to avoid adhesion to the PDMS polymer. In a swift, single motion, the spatula is dragged across the templates, starting from the end with PDMS. This allows the PDMS to be coated more uniformly across the wafer at the same width as the template. Since our template has a slightly smaller radius than the wafers themselves, one shortcoming of this method is that the wafer edges are not entirely coated in

¹Thickness measurements for the blade coating template and PDMS layer are taken with an EZ Cal Caliper, with an uncertainty of ± 0.1 mm (100 μm).

this process. Alternate coating methods are discussed in Chapter 5, but were insufficiently precise in their current state for the purposes of this project.

4. **PDMS Curing:** Once the PDMS has been coated over the wafer surface, the wafer is set on a hot plate at 100°C for 45 minutes. Heating allows the PDMS to solidify, adhered to the wafer surface. Although this "curing" can take place if left to sit at room temperature for a long duration (24 hours), rapid curing via heat ensures that the thickness at the time of coating is maintained.

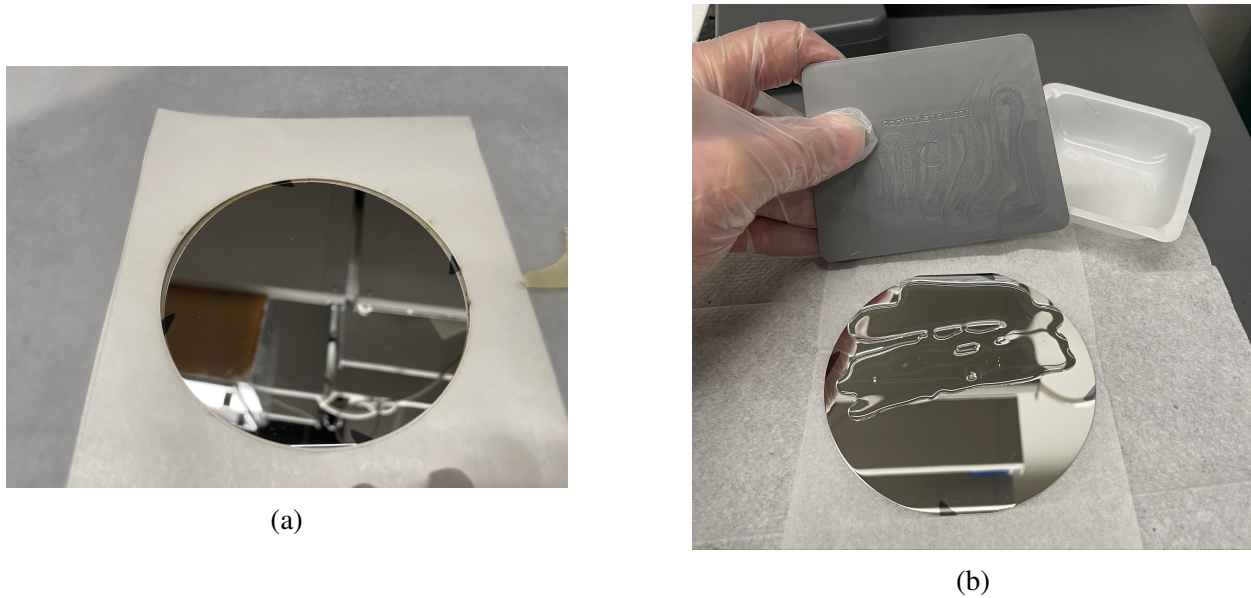


Figure 3.3: (a) Silver-coated silicon wafer prior to PDMS blade-coating, with compressed paper template applied; (b) PDMS deposited on a wafer prior to blade coating. Teflon spatula shown for scale.

Figure 3.4 illustrates the stacked layers of the silicon-based and silica-based thermal emitters, respectively. Layers are not drawn to scale, and are intended to show general structure within the emitter. Following the PDMS application, the wafers are ready to be tested in outdoor environments.

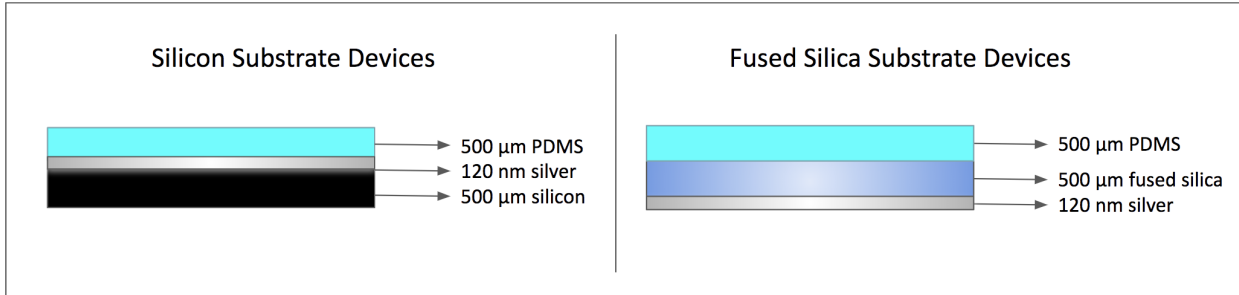


Figure 3.4: Illustrations of cross section for the silicon-based (left) and fused silica-based (right) passive cooler thermal emitters with layers of silver (Ag) and polydimethylsiloxane (PDMS). PDMS is shown in light blue for emphasis but is transparent in the visible. Layers are not drawn to scale.

3.2 Developing an Experimental Set-Up

The primary experiments in this thesis entail setting our thermal emitters in a rooftop environment in Claremont, California in early spring to evaluate their passive cooling potential. This section describes both the method of our temperature data collection, as well as the experimental design.

3.2.1 Constructing a Housing Apparatus with Minimal Parasitic Effects

Since we are most concerned with the radiative dynamics exclusive to our thermal emitter wafers, it is important that the wafers themselves be housed in structures that minimize parasitic heating from convection and conduction in the surrounding environment. This requires using lightweight materials that themselves experience minimal solar absorption. Also required is a set-up to record temperature data for our thermal emitters for multi-hour durations. This section describes the development of the final thermal emitter as well as our temperature logging set-up.

3.2.1.1 A Petri Dish Prototype

The first prototype of our cooling apparatus was constructed in the fashion of Kou et al., using off-the-shelf materials to reduce parasitic heating and isolate energy exchanges between the thermal emitter and surroundings as much as possible [12]. The thermal emitter wafer is set in the

bottom half of a standard, three-inch diameter petri dish, on top of a polystyrene bed to minimize energy transfer between the wafer and the petri dish itself. The dish is elevated on three glass stirring rods, which minimize conduction between the petri dish and rooftop surface. A multimeter thermistor is wired through the petri dish and adhered to the back of the wafer with thermal conductive tape to measure the wafer temperature. This set-up is depicted in Figure 3.5.

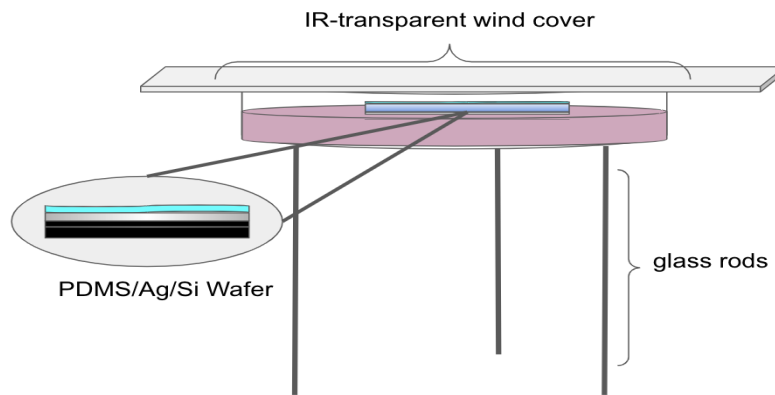


Figure 3.5: Passive cooling testing apparatus. A PDMS/Ag-coated wafer sits atop polystyrene thermal insulation within a petri dish covered with an IR-transparent wind cover. Wind covers are not used in the final testing due to their individual spectral properties, but warrant future investigation.

3.2.1.2 3D-Printed Stands

Although the petri dish design in our first prototypes has the benefit of being inexpensive and easy to construct, it suffers from a lack of stability, as well as a tendency for components such as the thermistors and wafers to shift. In our second prototype, which is used in our outdoor experiments, we instead 3D print wafer stands, using a fused deposition modeling printer. The stands are made from a lightweight, translucent polyactic acid filament which should be minimally absorbent of sunlight and thermally insulating. The polystyrene still sits snugly in the stand, allowing the wafer to be set on top. A small trough is cut into the polystyrene insulation to make room for a

temperature probe that can remain in contact with the back of the wafer. This set-up is depicted in Figure 3.6.

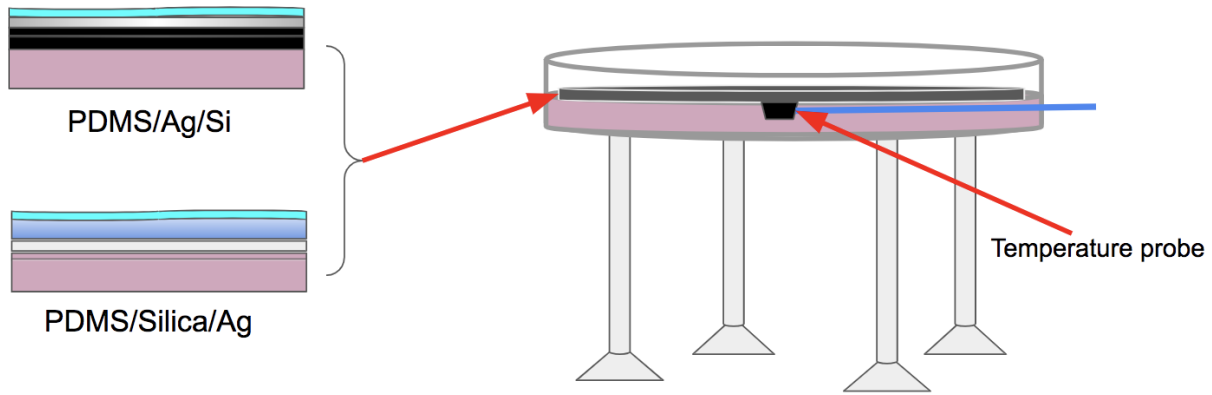
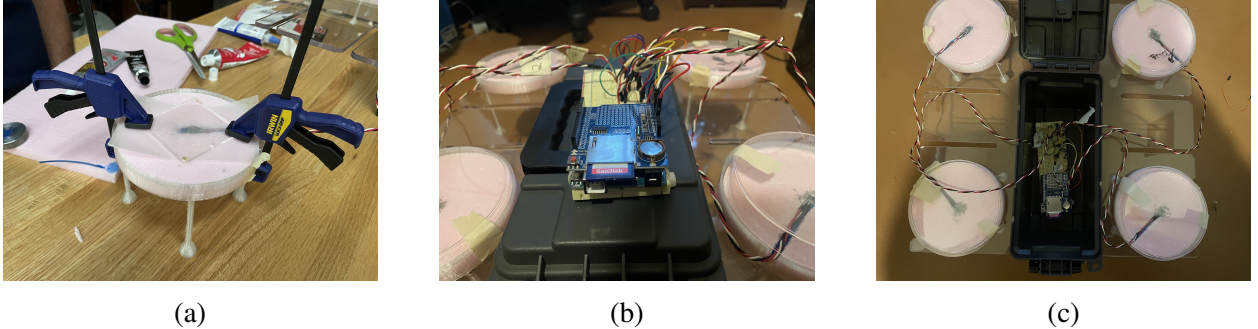


Figure 3.6: Schematic of a thermal emitter, housed in a 3D printed stand. Cross sections to the left indicate both types of wafers used in the thermal emitters, on silicon and fused silica substrates, respectively.

3.2.1.3 Taking temperature data

To assess cooling performance in our thermal emitters, it is important that we are able to collect temperature data for each wafer for several hours at a time, especially during hours of peak solar irradiation. For that reason, it is important to have a standalone temperature measurement apparatus. To achieve this, we construct a simple breadboard circuit using an Arduino micro-controller and data logger shield attachment. To measure temperature of the thermal emitters and experimental controls, we use TMP36 analog temperature sensors, which measure the change in a voltage drop across a diode which is directly proportional to change in temperature. The temperature sensors are nestled in the polystyrene insulation in each wafer stand and kept in contact with each wafer using thermal conductive paste (Figure 3.7a).

The temperature sensors are additionally soldered to wiring that plugs directly into the bread-



(a)

(b)

(c)

Figure 3.7: Testing apparatus components including (a) device stand in the process of setting a temperature sensor in the thermal insulation prior to testing; (b) close-up of the Arduino/data logger circuit; (c) bird’s eye view of the temperature circuit in the carrying box, wired to each individual device stand (without passive cooling wafers present).

board. Another set of wiring allows the output from the temperature sensors to be connected directly to analog pins on the Arduino Uno. However, instead of plugging directly into the microcontroller, we use a HiLetgo data logger shield that plugs into the digital and analog pins atop the Arduino. We then wire our temperature probes directly to the data logger, while still maintaining access to the full functionality of the Arduino. The Arduino is programmed to record the temperature data at each analog pin at a set time interval (we use both two-minute and one-minute intervals), which is written to a CSV file and stored on an SD card. To protect the circuitry in the outdoor testing environment, the breadboard, Arduino, and data logger are stored in a small carrying box, from which the temperature probe wires extend to the individual wafer stands. Also attached to the carrying box is a plastic carrying rack which can hold the wafer stands, enabling the entire apparatus to be mobile. Our experimental set-up is then ready to be tested in outdoor conditions.

3.2.2 Outdoor Experiment

We perform separate outdoor experiments to test radiative cooling performance in the silicon thermal emitter devices and the fused silica devices. In each experiment, four wafers stands are set in an outdoor rooftop environment for several hours of testing. We include the thermal emitter wafer with a PDMS/silver coating, a control with only silver, and another control comprised of a

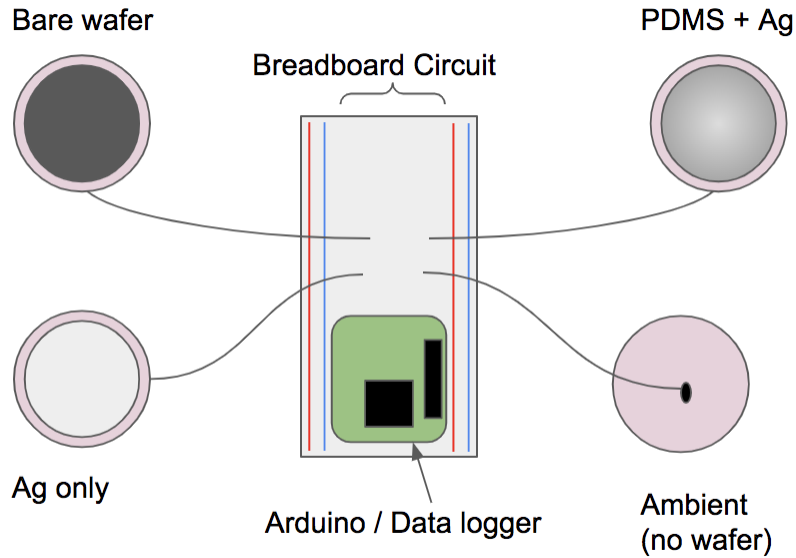


Figure 3.8: Experimental set-up and breadboard circuit used to log temperature data during outdoor experiments. In the final testing design, the ambient temperature sensor is shaded by a makeshift solar blocker to ensure the sensor is not heated directly by the sun.

bare wafer. We additionally include a stand containing only a temperature probe with no wafer, which is intended to measure the ambient air temperature. This array is detailed in Table 3.1. The specific orientation of our PDRC thermal emitters relative to the controls is additionally depicted in Figure 3.8.

Each experiment has two parts, testing first in daytime conditions and subsequently in nighttime conditions. Although we are primarily interested in daytime cooling, nighttime testing in the absence of sunlight provides important data to better distinguish the impact on cooling from the reflective versus emissive coatings in our thermal emitters. Daytime testing takes place during peak sunlight hours, which we define as extending from 10:00 am to 3:00 pm. This is influenced partly by duration of shade from surrounding structures in our testing environment.

Since we are less concerned with evaluating temperature comparisons during a specific time overnight, we collect data for a longer period. Although the duration of our experiments vary, we analyze data from a set time period from 10:00 pm to 6:00 am the following morning. Data in both

Device Type	Fused Silica Wafers (FS)	Silicon Wafers	Purpose
Ambient Temp	No Wafer	No Wafer	Provide a baseline ambient temperature measurement.
Control 1: Bare Wafer	FS Only	Silicon Only	Measure substrate temperature with no additional layers.
Control 2: Reflective Wafer	FS + Silver	Silicon + Silver	Compare temperature changes with the reflective silver surface applied.
PDRC Thermal Emitter	FS + Silver + PDMS	Silicon + Silver + PDMS	Measure the cooling potential with both the reflective silver surface and the emissive PDMS coating.

Table 3.1: Comparison of PDRC cooling beds to experimental controls

daytime and nighttime trials are recorded in one-minute intervals via the Arduino data logger.

3.3 Summary

This chapter describes the fabrication process for two types of thermal emitters, as well as the construction of our experimental apparatus for outdoor testing. Also discussed are the experimental set-up, including temperature-logging circuitry and the controls developed alongside the passive cooler devices. Chapter 4 details the results and implications of our testing and also details more of the progression of work on this project that led to the final version of our thermal emitters and set-up.

4. RESULTS AND DISCUSSION

A primary objective of this project is to construct low-cost, passive radiative cooling devices that can cool to below-ambient temperatures in outdoor, rooftop environments. This chapter explores the results of these experiments, which measure the cooling performance of our passive cooling devices on a rooftop in Claremont, CA in early spring. First, we outline results from our two primary tests, separately comparing the temperatures of our silicon and fused silica devices to experimental controls in clear daytime and nighttime conditions. We initially find that sub-ambient passive cooling occurs in the fused silica devices, but not in the silicon devices. We predict that this could be due to an insufficient thickness in the layer of PDMS in the silicon devices. Results from a third experiment are presented, in which we modify the PDMS polymer thickness in the silicon emitter and subsequently observe successful sub-ambient cooling in the silicon passive cooler as well.

This work has seen multiple iterations of each component of our devices and experiment design. In addition to the end results of our rooftop experiments, this chapter also documents the progress to realizing the final experimental set-up with indications for future improvements. This includes a temperature calibration experiment, the purpose of which is to ensure measured cooling is not due to inherent offsets in our temperature sensors.

4.1 Rooftop Experiment Results

One of the goals of this project is to compare the performance of passive cooling surfaces built on silicon substrates with those on fused silica substrates. Our experiments therefore consist of two experimental set-ups for each of these wafer substrates. Each set-up consists of a complete device with both silver and PDMS layers. In addition, we simultaneously test three controls: a wafer layered with only silver, a bare wafer with neither silver nor PDMS, and a standalone temperature sensor to measure the ambient air temperature.

Our testing is conducted in an outdoor rooftop environment to maximize exposure of the sur-

faces to the sky, with minimal solar blocking from surrounding objects (Figure 4.1). For each experimental set-up, a trial is conducted for several hours around midday to capture temperatures during maximum sunlight, in addition to a trial conducted overnight to compare the temperatures of the wafers in the absence of sunlight. Relative temperature differences are reported with a standardized uncertainty of ± 1 °C based on measured fluctuations in all four temperature sensors. Plots of each of these trials, along with the discussion of the results, are presented below. In all experimental figures excluding temperature calibrations, the ambient temperature is shown in blue, the passive cooling device is shown in orange, the silver control is silver, and the bare wafer control is yellow.



Figure 4.1: Passive cooling testing set-up in rooftop environment. A make-shift solar blocker is constructed from a box lid to ensure the ambient temperature probe remains in the shade. Experimental controls are at the top of the image and the PDRC device is shown at the bottom.

4.1.1 Experiment 1: Silicon Devices

Figures 4.2 and 4.3 show the results from both the daytime and nighttime temperatures for the silicon wafers. We see in both the daytime and the nighttime testing that the PDMS-coated wafer

essentially mirrors the ambient temperature, but does not achieve substantial cooling below the ambient level. We do, however, observe cooling in the devices relative to the other experimental controls.

4.1.1.1 Silicon Daytime Experiment

In the daytime results, the temperature of the silicon wafer control increases sharply and remains elevated above ambient throughout the duration of the trial. This is not unexpected, as the darker silicon wafer is highly absorbent of solar radiation, which causes the wafer temperature to increase. Similarly, the silver-coated wafer also maintains a temperature consistently above ambient, although it is still substantially lower than the bare silicon wafer. This also makes sense, because although the silver coating will reflect much more solar irradiance than the bare silicon wafer, the silver-coated silicon is not expected to be highly emissive in the infrared. In contrast, PDMS-coated surface maintains an average temperature of approximately 19.3 °C below the silicon wafer control and 5.5 °C below the silver-coated silicon control, suggesting that the PDMS polymer coating does enable some degree of radiative cooling compared with its control counterparts. However, the emitter does not cool noticeably relative to ambient air temperatures.

The spike in ambient temperature around 2:30 pm during the daytime testing is likely due to exposure of the ambient temperature probe to sunlight. It is expected that a temperature probe measuring ambient temperature will be left in a shaded area, but accidental exposure to sunlight can cause the temperature reading to be much higher than the ambient surroundings.

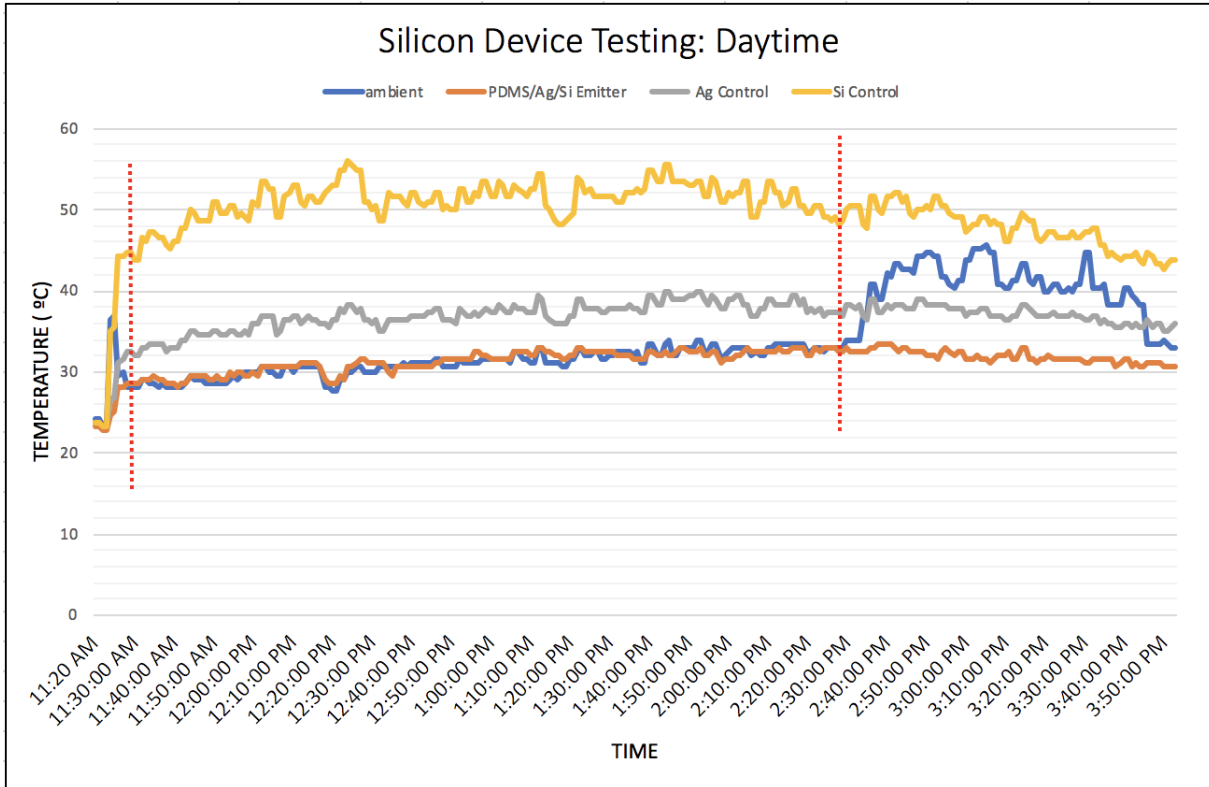


Figure 4.2: Temperature data for silicon wafer set-up from 11:20 am - 3:50 pm in mid-March in Claremont, CA. Dotted red lines mark peak daylight hours for which temperature comparisons are calculated. The spike in ambient temperature around 2:40 pm is due to exposure of the temperature sensor to sunlight.

4.1.1.2 Silicon Nighttime Testing

The nighttime silicon testing does not exactly mirror the daytime results in the inter-wafer temperature comparisons. The temperature of the thermal emitter drops consistently below the ambient temperature by 2.7 °C, likely due to strong blackbody radiation in the atmospheric window. However, two somewhat surprising results emerge: first, the bare silicon wafer cools to below-ambient temperatures as well, maintaining a comparable sub-ambient temperature difference of 3.0 °C compared to the thermal emitter. The bare silicon wafer may be more effective at nighttime cooling for the same reason it absorbs so much heat during the daytime. As shown in Equation 2.4, strong absorptivity in silicon over solar wavelengths means that silicon has also has a high emittance, which may explain the higher temperature reduction in temperature at night

without any radiation to absorb from the sun. The second unexpected result is that the silver wafer maintains a consistently higher temperature than ambient throughout the nighttime trial. Although we expect the device with PDMS to be cooler than the control with only silver, it is unclear why the silver wafer appears to retain more heat than both the bare silicon wafer and the the ambient air.

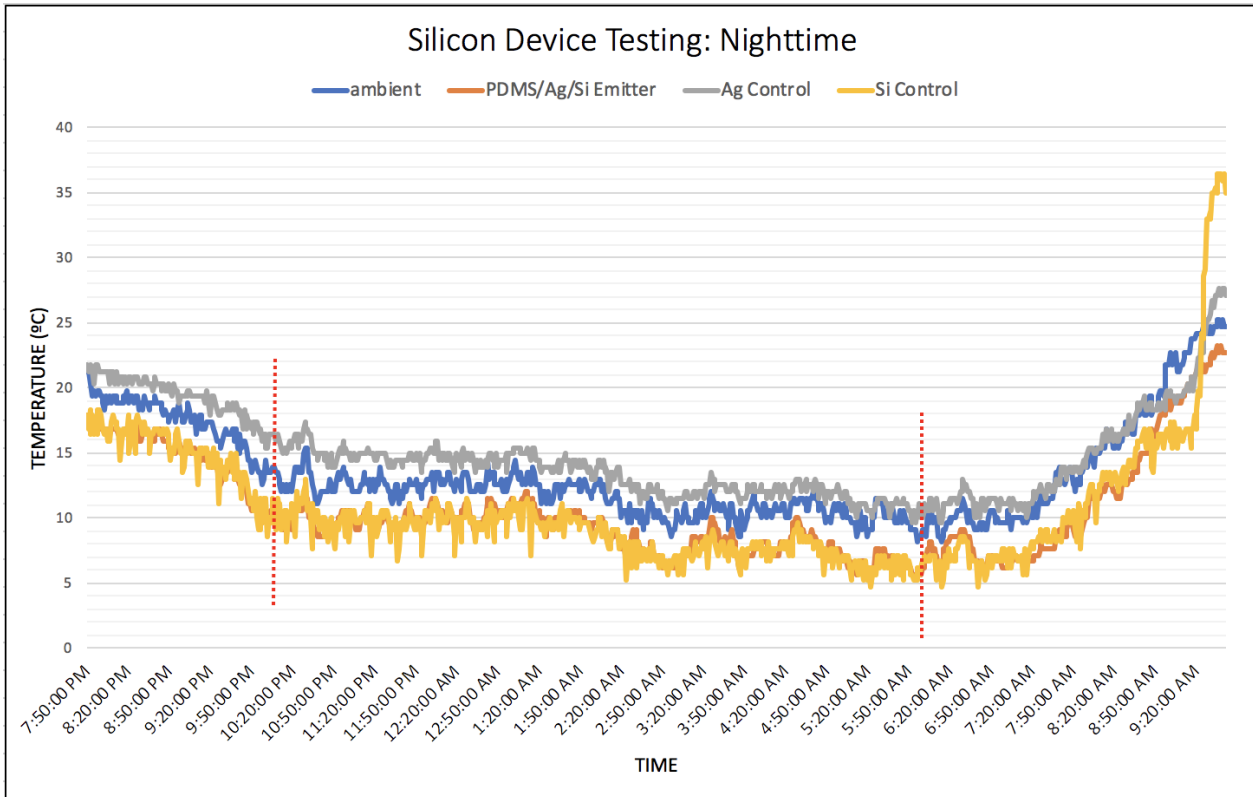


Figure 4.3: Temperature data for silicon wafer set-up from 8:00pm - 9:30am the following morning in mid-March in Claremont, CA. Dotted red lines denote the time interval over which temperature comparisons are calculated. The increase in temperature in early morning hours and the spike in the silicon control temperature indicate sunrise. Thermal emitter and silicon control temperatures drop to 2.7 °C and 3.0 °C below ambient.

The outdoor temperature data from the initial silicon-based devices thus demonstrates partial radiative cooling. The PDMS-coated devices do not achieve sub-ambient cooling in the daytime but maintain temperatures below their control wafer counterparts. We do observe below-ambient

cooling at night, although the effect is essentially mirrored by the bare silicon wafer control. The silicon device experiment is repeated with varying PDMS thickness, described in subsection 4.1.3.

4.1.2 Experiment 2: Fused Silica Devices

In addition to outdoor trials using silicon wafers for both passive cooling surfaces and controls, we repeat the experiment using fused silica substrates. Our approach is based on that of Kou et al. [12]. We again conduct an experiment starting and ending several hours before and after midday to capture the effect of peak sunlight, as well as a longer trial running overnight from mid-afternoon to mid-morning of the following day.

4.1.2.1 *Fused Silica Daytime Testing*

Figure 4.4 depicts the temperature trends in the daytime fused silica wafer experiment. It appears as though the bare fused silica wafer control rises to a temperature well above ambient, similar to the bare silicon wafer in the previous experiment. However, it is worth noting that the bare fused silica wafer is transparent over much of the solar spectrum. Since the temperature sensor is attached to the back of the wafer, it is difficult to determine how much of the temperature increase can be attributed to the wafer absorbing radiation, as opposed to direct solar heating of the temperature sensor itself.

More importantly, however, we observe sub-ambient cooling in the device with silver and PDMS layers throughout the daytime experiment. Our experimental device averages temperatures 3.5°C cooler than ambient air temperatures during peak sunlight, which is a highly-desirable result. Additionally, in contrast to the silicon wafer experiments, the silver-coated wafer does not give rise to substantial temperature increases, and in fact averages a below-ambient cooling of 1.3°C . This degree of cooling is nearly within the measure of uncertainty for our comparisons ($\pm 1^{\circ}\text{C}$), but the difference from the silicon control may suggest that the substrate selection may play a role in the degree of cooling that occurs. The order of the layers within our devices could also be a factor since the fused silica devices have the silver reflective coating on the back of the wafer, opposite to the PDMS.

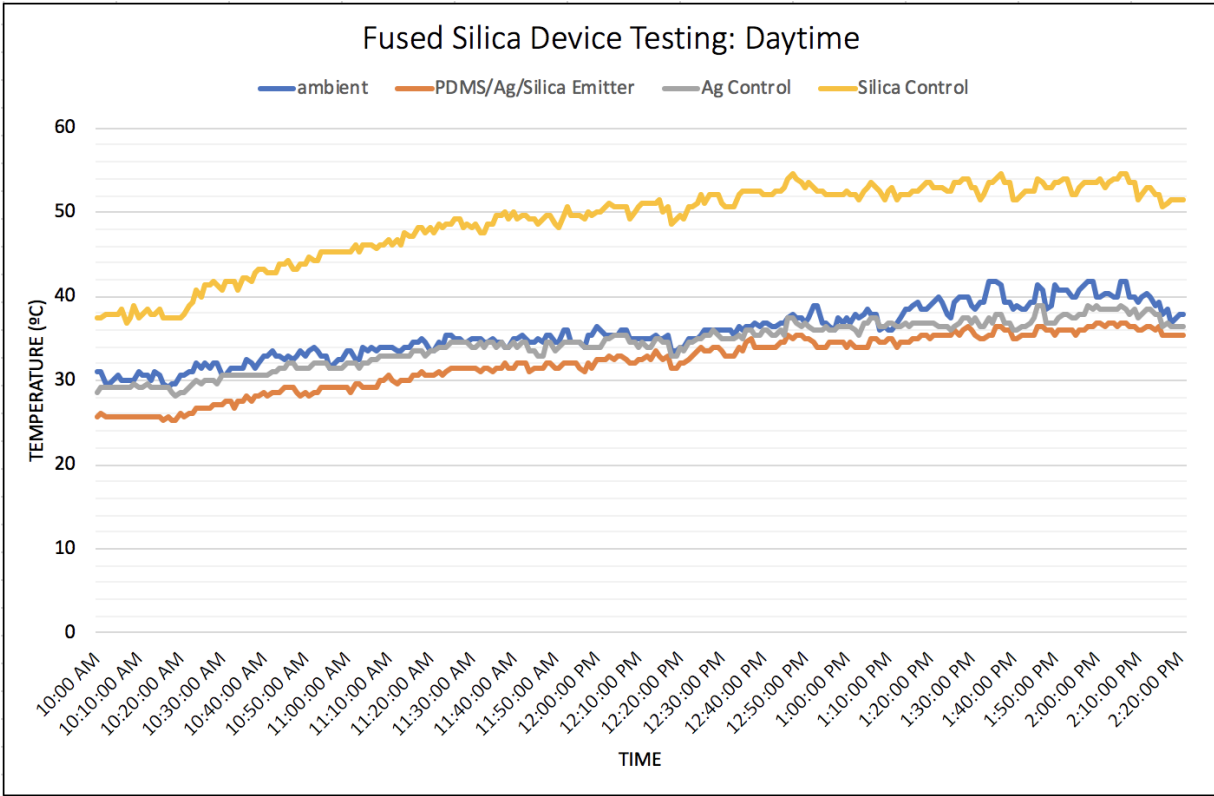


Figure 4.4: Temperature data for fused silica wafer set-up from 10:00am - 2:20pm in mid-March in Claremont, CA. The fused silica passive cooling device averages 3.5 °C below ambient temperature (orange line relative to blue).

4.1.2.2 Fused Silica Nighttime Testing

We observe similar results in the nighttime trial (Figure 4.5). First, we again see that the thermal emitter device maintains a consistent temperature below ambient, approximately 3.3 °C. This margin is comparable to the degree of cooling than in the daytime, although it is worth noting that the nighttime trial is longer in duration. Second, we note that the silver-coated control does not appear to retain additional heat, as appears to be the case in the silicon experiment. Instead, the silver control essentially mirrors the ambient temperature throughout the night, again suggesting that the substrate material plays some role in temperature variability. Additionally, the bare fused silica wafer control also cools below ambient, essentially following the PDMS-coated wafer. In this case, we can assume more confidence in the fused silica control temperature, as there is no

sunlight to heat the temperature probe excessively.

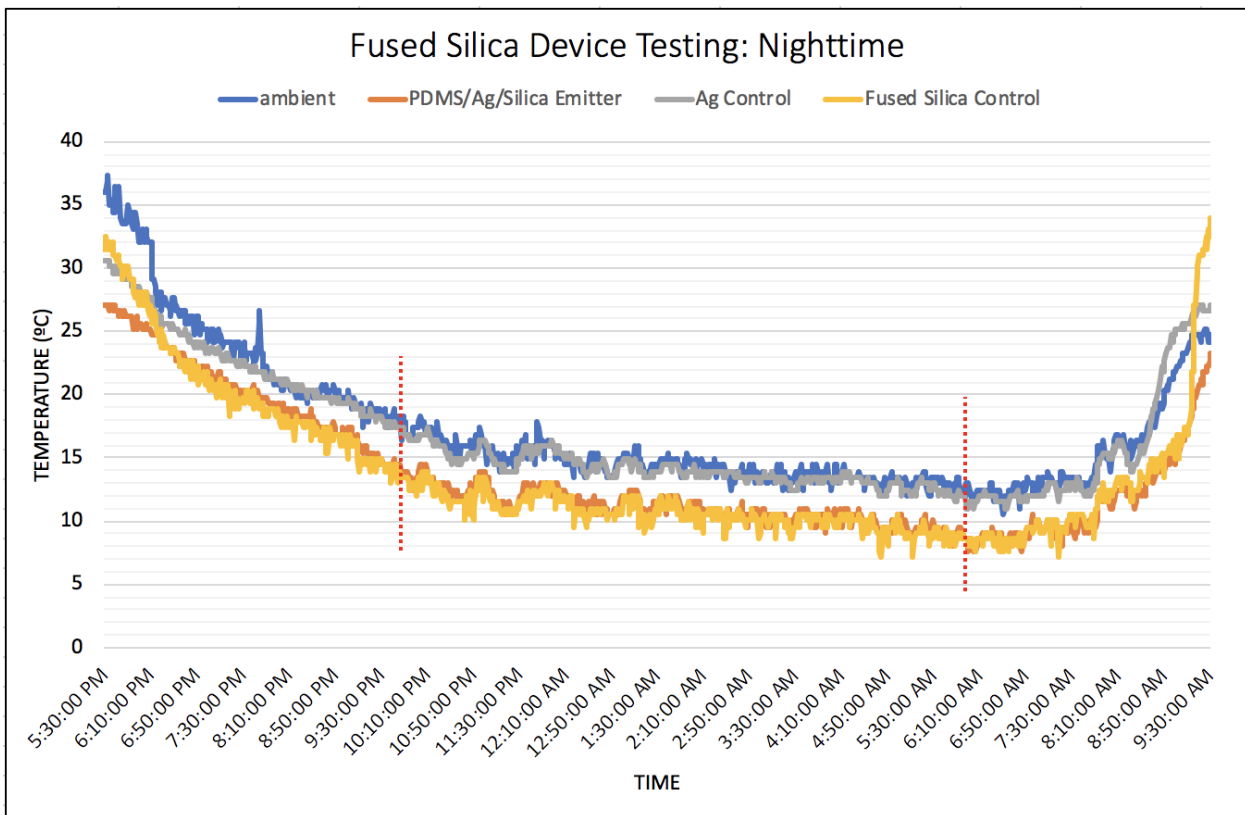


Figure 4.5: Temperature data for silicon wafer set-up from 3:45pm - 10:30am in mid-March in Claremont, CA. The passive cooler (orange) averages 3.3 °C below ambient temperature (blue).

4.1.3 Experiment 3: Adapted Silicon Devices

4.1.3.1 Varying PDMS Thickness

Results from the two outdoor experiments with silicon and fused silica devices suggest that the fused silica devices achieve a higher degree of passive cooling. However, one key difference in the set-up for these experiments is the method of coating PDMS on the devices. In the silicon experiments, we use a spin-coating method to deposit PDMS onto the wafers at a $100 \mu\text{m} \pm 40 \mu\text{m}$. In the fused silica experiments, we use the blade coating method described in Chapter 3. This coats the PDMS at a thickness of $500 \mu\text{m} \pm 100 \mu\text{m}$. Although more susceptible to non-uniformity, the

blade coating process enables us to coat the PDMS at thickness levels the spin-coater is not able to achieve. We therefore repeat the experiment in Section 4.1.1 with our silicon wafers, but instead apply a blade-coated PDMS layer of $500 \mu\text{m} \pm 100 \mu\text{m}$ to our experimental device. Results are presented in the following sections.

4.1.3.2 Silicon Retrial Daytime Testing

The daytime results for the adapted silicon thermal emitter with higher PDMS thickness show a larger degree of passive cooling than the original versions (Figure 4.6). We again see that the silicon and silver controls rise to elevated temperatures relative to ambient. Instead of tracking the ambient temperature, however, the passive cooler device drops below ambient air temperature for the duration of the experiment. The thermal emitter remains 3.2°C cooler than ambient and 20.9°C cooler than the silicon control during peak sunlight hours. This degree of sub-ambient cooling is slightly less than the fused silica device (3.5°C) but is much higher than in our initial silicon experiment, in which the thermal emitter and ambient temperatures were nearly identical (< 0.5°C average temperature difference). This suggests that the thicker coating of PDMS may enable a higher degree of daytime cooling by emitting more heat over mid-infrared wavelengths.

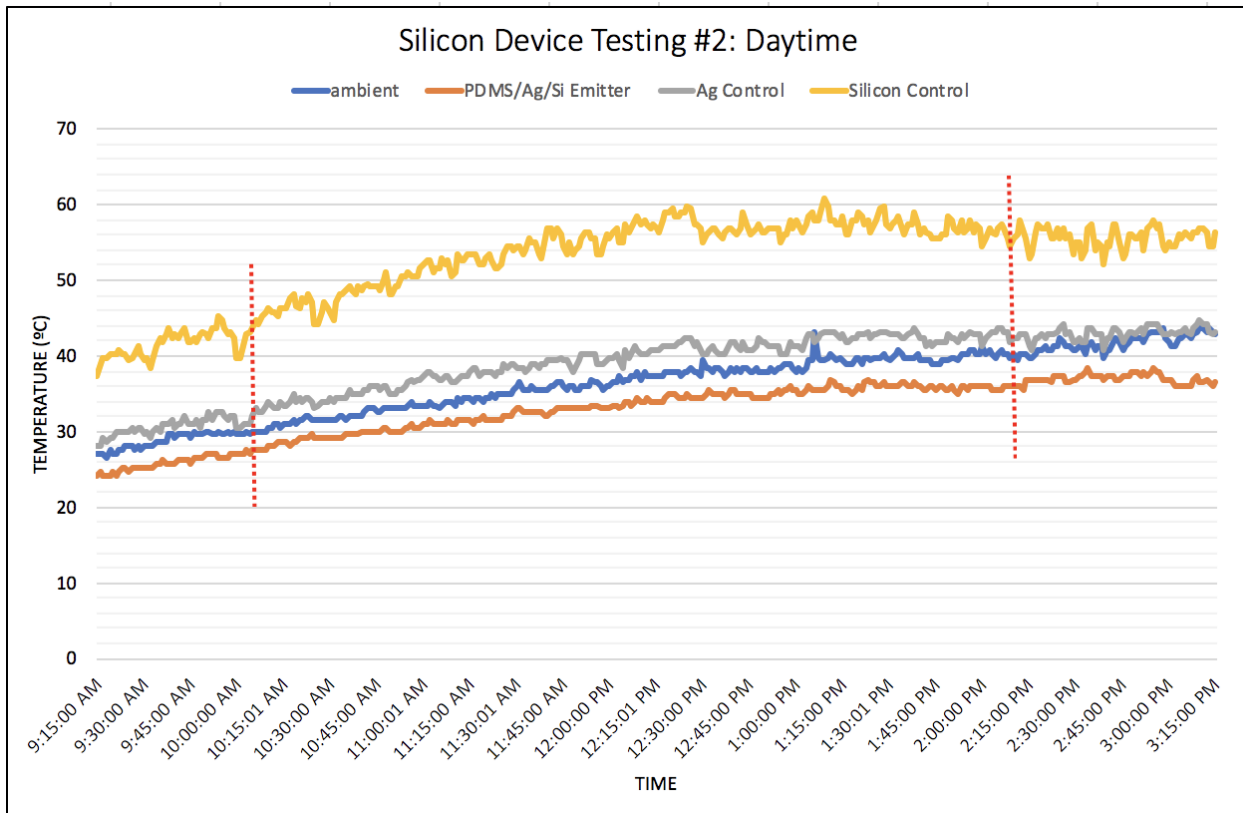


Figure 4.6: Temperature data for the adapted silicon wafer set-up with thicker PDMS, from 9:15 am to 3:15 pm in early April in Claremont, CA. Dotted red lines denote peak sunlight hours. The passive cooler maintains an average temperature below ambient air of 3.2 °C and 20.9 °C below the silicon experimental control.

4.1.3.3 Silicon Retrial Nighttime Testing

Despite the increased thickness of PDMS in our adapted silicon device, the nighttime results in the retrial silicon wafers appear very similar to the first nighttime experiment with silicon wafers (Figure 4.7). The thermal emitter maintains an average temperature below ambient by 3.4 °C. The silicon control seems to cool slightly more than the thermal emitter, averaging temperatures below ambient by 3.7 °C. However, this margin is generally within the ± 1 °C margin of uncertainty. We note also that the degree of cooling in both the thermal emitter and silicon control in this experiment is only around 0.5 °C more than the original silicon nighttime experiment, which is also within the margin of uncertainty. This is somewhat unexpected, as it suggests that an increase in

the thickness of PDMS is primarily beneficial for daytime cooling, but does not provide substantial cooling benefits in nighttime conditions.

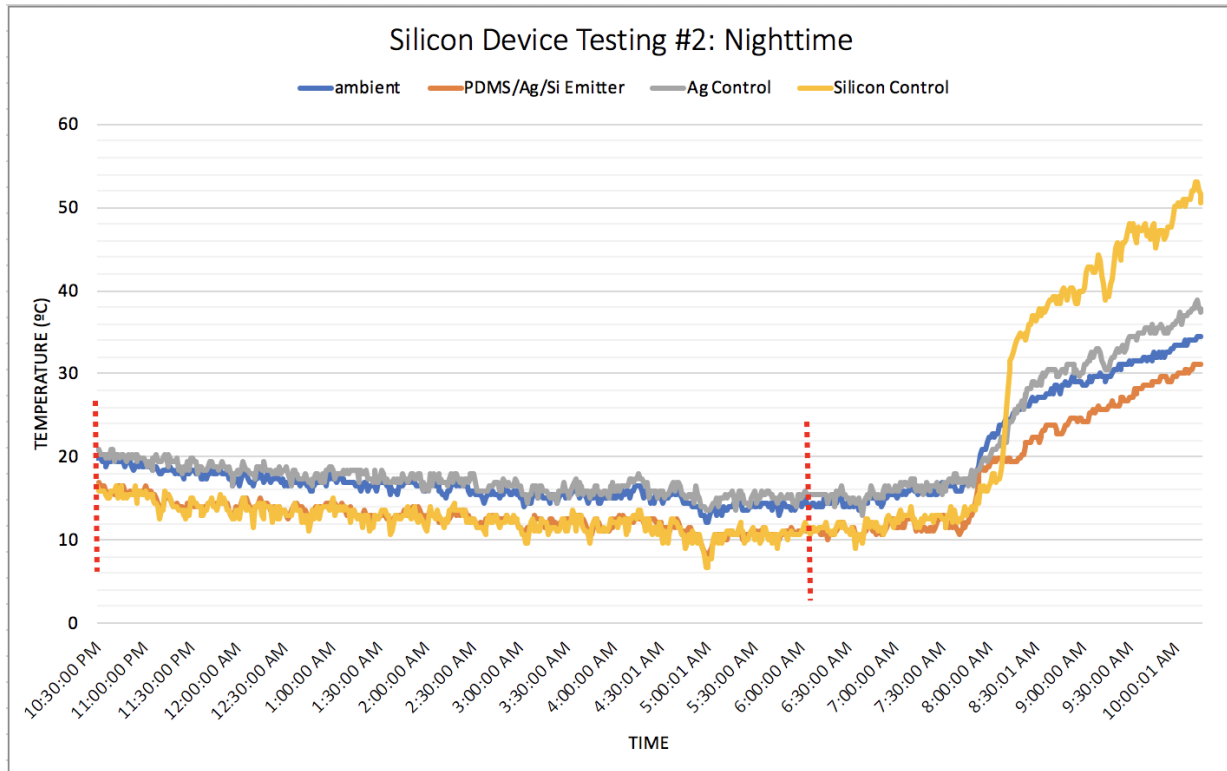


Figure 4.7: Temperature data for the second silicon wafer set-up from 10:30pm - 10:00am in early April in Claremont, CA. Below-ambient occurs for the thermal emitter and silicon control by 3.4 °C and 3.7 °C, respectively.

4.1.4 Discussion

Our results suggest that our experimental devices are most effective for daytime radiative cooling, and that the thickness of the polymer coating applied to the surface of the thermal emitter plays a role in its cooling potential. Our first experiment using silicon wafer substrates demonstrates "above-ambient cooling" during the daytime, maintaining an average temperature below the silicon and silver controls but not below ambient air temperature. The emitter and silicon control both achieve a noticeable degree of below-ambient cooling during the nighttime testing of

approximately 3 °C.

In our next experiment, the fused silica devices achieve sub-ambient cooling during both the daytime and nighttime trials, by 3.5 °C and 3.3 °C, respectively. The thermal emitter device also maintains temperatures below the experimental controls. Although the use of a fused silica substrate may play a role in this higher degree of cooling compared to the silicon device, we note that the fused silica device also has a substantially thicker coating of the PDMS film on the wafer surface. As a result, we repeat the silicon experiment with a layer of PDMS nearly five times as thick as the original to match the fused silica device.

Repeating the silicon device experiment with a thicker PDMS layer does result in more cooling, allowing the thermal emitter device to reach below-ambient temperatures by 3.2 °C and 3.4 °C during daytime and nighttime testing, respectively. This suggests that the *thickness of the PDMS layer is a key component of daytime cooling*, likely because of the high emissivity of PDMS over atmospheric window wavelengths.

In all three experiments during the nighttime trials, we note that the bare wafer control reaches comparable temperatures to the thermal emitter device. This is somewhat unexpected, suggesting that, while the PDMS coating appears to substantially enhance the device emissivity during the daytime, it does not appear to greatly influence the nighttime temperatures. At the same time, while the bare wafer controls cool off considerably at night, they consistently heat up to nearly 20°C above ambient during the daytime. This underscores the importance of the silver layer in our devices, which reflects much of the solar radiation that would otherwise be absorbed. Therefore, in both the silicon devices and fused silica devices, we determine that the reflective silver layers and emissive PDMS layers are both integral to achieving sub-ambient passive daytime radiative cooling.

In our outdoor experiments, we have conducted preliminary explorations into the role of PDMS thickness in device performance, as well as comparisons between different substrate materials for passive cooling devices. Our results reaffirm the importance of selecting materials for passive coolers that reflect high amounts of solar radiation and are highly emissive over mid-infrared wave-

lengths. While our devices do not achieve the same level of cooling as results from the literature [7][12], we note that our devices do not actively minimize convective heating, which could be a factor in reduced cooling capacity. This is discussed further in subsubsection 4.2.2.2. Additionally, while the margin of sub-ambient cooling is not extreme, the cooling relative to experimental controls of nearly 20 °C is very notable for potential applications in rooftop coatings or other surfaces that are both exposed to substantial solar absorption.

4.2 Progression of Experiments

While our end goal is to evaluate the temperatures of our passive cooling devices, a substantial part of this project has consisted of developing the device fabrication process and experimental set-up. We therefore document the progression of our work in each of these areas in this chapter, in addition to the rooftop experimental results presented above. The current iteration of our outdoor experimental set-up consists of a four-device array: one experimental thermal emitter coated with reflective silver and an emissive PDMS polymer, two wafer controls, and one ambient temperature sensor. The four devices are connected to an Arduino data logger, and the entire apparatus is set on a rooftop environment with maximal sky exposure. This set-up is described in detail in Chapter 3. Here, we discuss the iterations of our initial testing and previous experimental set-ups, including pitfalls encountered and modifications made before realizing the current experimental design. This is included both to document the progression of this project, as well as to serve as a reference for future researchers.

4.2.1 Initial Testing

Our initial experimental set-up served primarily as a proof-of-concept test of our ability to measure the temperature of our wafers in an outdoor environment (Figure 4.8). Initial prototypes consisted only of the silicon-based devices and did not include the fused silica counterparts. Silicon wafers are cleaved into single square-inch pieces before being set on a bed of polystyrene foam insulation in a three-inch diameter petri dish. The dish is elevated on three glass stirring rods with a thermistor read by a multi-meter connected to the back of the wafer with thermal conductive tape

to measure the temperature.



Figure 4.8: Original petri dish experimental set-up with silicon wafer thermal emitter devices. Multimeter thermistors are used to measure device temperature.

Two issues are made immediately clear with this set-up. First, using multimeters to measure the device temperatures is fast and reliable, but there is no way to automatically log the temperature data, nor a method of temperature standardization across each probe. Second, the rigidity of the wires from the multimeters physically elevates the wafers, such that the backside is no longer in contact with the foam insulation. These drawbacks are compounded by the inherent instability of supporting the dishes with stirring rods. As a result, in addition to the scientific goals of this project, an additional goal has been to construct an experimental set-up that has more physical stability, with a standardized means to log reliable temperature data.

4.2.2 Experimental Set-Up Modifications

4.2.2.1 Wafer Housing

Several adaptations were made to the initial experimental set-up to reach the current iteration described in Chapter 3. First, with the addition of the silica wafers, we standardized the device size to four-inch diameter circular wafers. This is done so that we can have a precise comparison between the silicon and fused silica sets, without having to cleave any wafers, which can be an imprecise process. A consistent wafer size also allowed us to make more stable and consistent structures to house the devices. Instead of using off-the-shelf petri dishes, we 3D printed 4.5-inch diameter trays that stand at a height of four inches off the ground. We use the same polystyrene foam insulation as the first experimental set-up, which fits snugly into the holding tray to minimize parasitic heating from the below surface on which the trays stand.

4.2.2.2 Temperature Probes

We log temperature data from the ambient control and wafers using TMP36 thermal sensors, connected to an Arduino Uno integrated circuit. Although the TMP36 is relatively responsive to temperature variation, we found several areas that required additional testing and modification.

First, we ran into an issue with the ambient air probe exposed to sunlight. In our preliminary tests with the new wafer housing and Arduino set-up, three TMP36 sensors were put in contact with the thermal emitter and two control wafers, while one was left exposed to open air. The temperature readings from this ambient air sensor, however, reached up to 50 °C (122 °F) which is inaccurate and implausible. We reason that, if exposed to direct sunlight, the TMP36 itself heats up and registers a very high temperature, as opposed to measuring the surrounding air temperature. To fix this, we add a solar-blocking shade cover to ensure that the ambient air probe is protected from the sun, while still exposed to the surrounding air. This entails setting the ambient sensor device in a small cardboard box, the lid of which is propped open to block sunlight from hitting the sensor. This approach was successful in improving the ambient air temperature measurements, which were cross-referenced with an external thermometer at the beginning of each experiment

and were consistent within ± 1.5 °C.

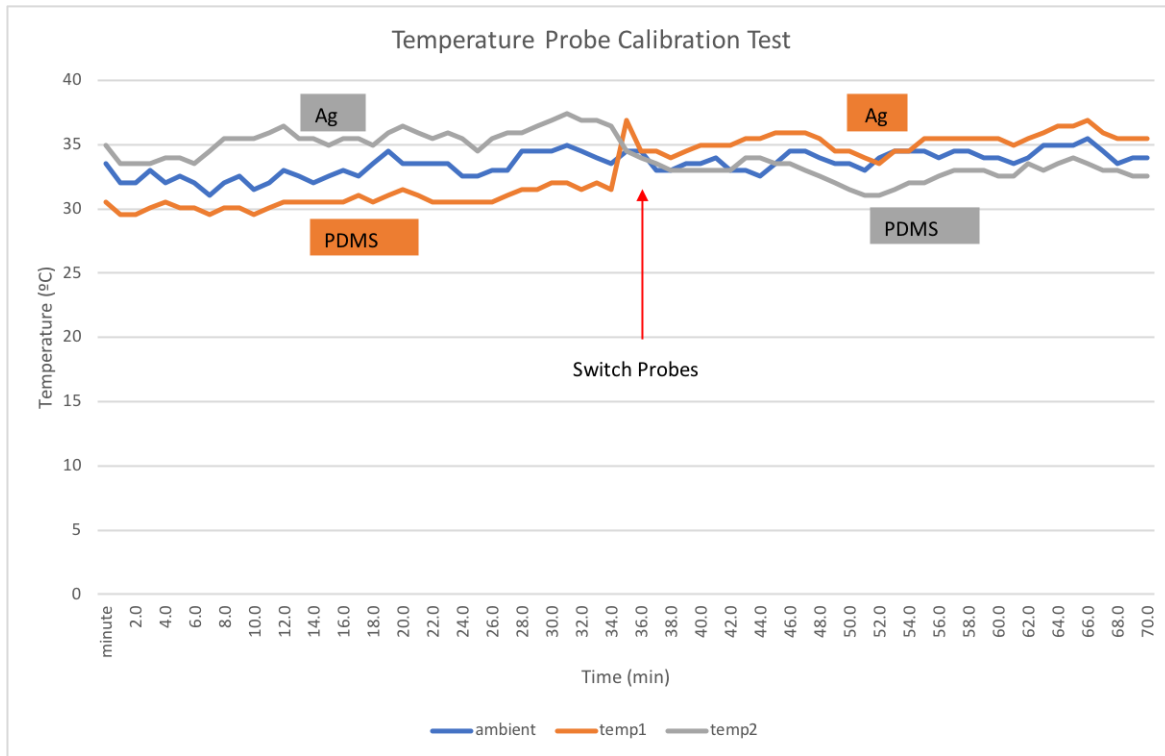


Figure 4.9: Checking the agreement of individual temperature probes with fused silica wafer set-up. Temperature sensors for the passive cooler device and silver control are switched after a half hour. The step-wise shift in the data shows that the temperature probes are sensitive to the relative wafer temperatures.

Offsets between individual temperature sensors are also taken into consideration. The TMP36 lists a precision of ± 1.0 °C at temperatures over 25 °C and ± 2.0 °C for temperatures less than 25 °C. This is a high degree of uncertainty compared to our level of cooling, so it is important to ensure that the results that we observe are not due to inherent offsets between individual temperature probes. We do not calculate an individual calibration coefficient for each sensor in our experiments, but we do perform multiple comparative experiments with the sensors to test their relative performance.

First, we observe in our measurements that the individual uncertainty in the precision of each

probe is close to ± 0.5 °C, regardless of the temperature being above or below 25°C. The range of measurements for all four sensors in a controlled environment is ± 1.0 °C, which is the uncertainty that we report in our temperature comparisons. Thus, while the specifications for the TMP36 sensors list an uncertainty of ± 2 °C at temperatures < 25 °C, we experimentally verify that the sensors are more precise. This reduces our individual probe uncertainty, but we are still left with a question of the relative measurements. From our results for the fused silica wafers, we anticipate that the wafer coated with PDMS will cool to temperatures lower than the wafer coated with just silver. We ran an experimental trial for approximately one hour, switching the probes connected to the control wafer coated with only silver and the thermal emitter with silver and PDMS halfway through testing (Figure 4.9). The results show that the two temperature profiles flip after this switch, indicating that the sensors are sensitive to the temperature differences in our wafers.

This experiment is repeated with all four temperature sensors using the silicon wafer set-up, shown in Figure 4.10. The sensors are rotated every forty minutes to determine if the relative temperatures of the wafers remains intact. The data in Figure 4.10 show that after each rotation, the temperatures of each device are in line with what we expect relative to each other and the ambient temperature. Thus, while we leave individual sensor calibration to future work, we conclude that the cooling we observe in our experiments is not substantially influenced by inherent offsets in our temperature sensors.

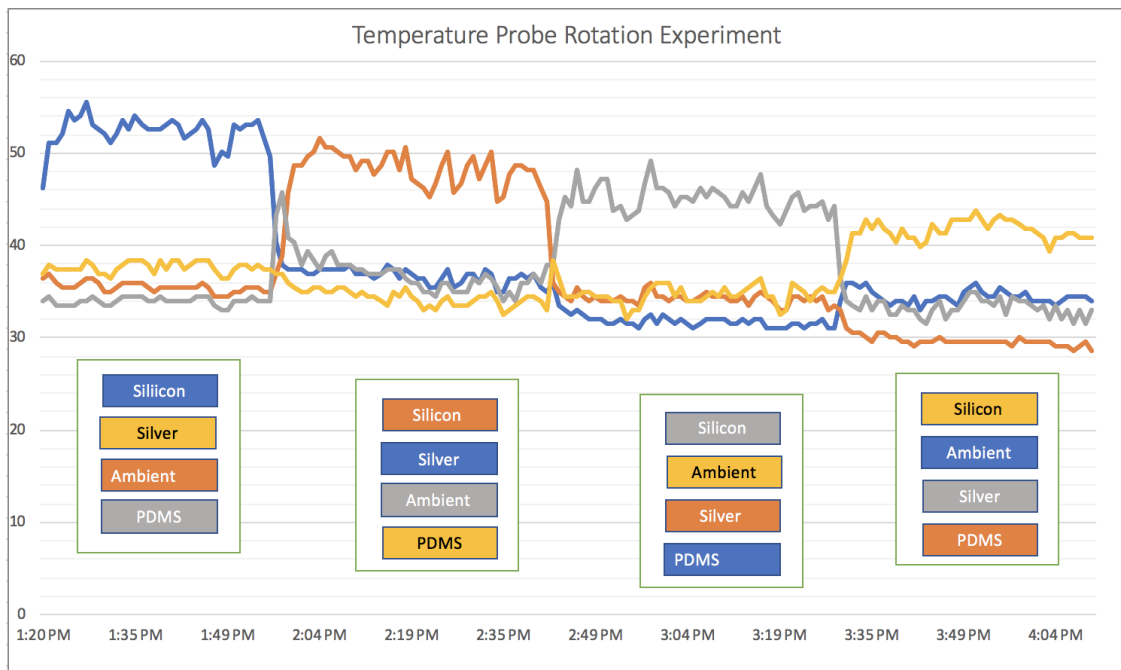


Figure 4.10: Cross-referencing the sensitivity of all four temperature sensors. Sensors are rotated every forty minutes with four total iterations. The plotted data and individual keys in the figure for each trial show that the expected relative temperature differences remain constant throughout the experiment.

4.3 Device Construction

The design of the thermal emitters used in our experiments is intended to be relatively simple. Our silicon and fused silica substrates have deposited on them a layer each of silver and PDMS. Depositing silver onto each substrate is a straightforward process, using a thermal evaporator to coat the substrate at a thickness of $120\text{ nm} \pm 3\text{ nm}$. Layering PDMS has proven to be a more complicated process. This is due in part to the high viscosity of PDMS, as well as its tendency to cure to substrates at room temperature. In our initial testing with smaller cleaved wafers we were able to blade coat PDMS over the square wafers at a specified thickness using commercial scotch tape as a template. This is done by applying tape to the edges of the wafer, and following the blade coating process described in Chapter 3.

Since adapting our process to use larger, circular wafers, we have been working to coat the PDMS uniformly on the wafer substrates using a spin-coater. Spin-coaters are intended to apply

materials to a substrate at a uniform thickness based on a specified revolutions per minute (RPM) rate and spin time. Using previous literature documentation for spin-coating PDMS, we attempted to coat our substrates at a thickness of 100 μm . However, even with several attempts made to modify the spin duration as well as RPM, we failed to achieve a sufficiently high thickness in our PDMS layer. This could be a result of the PDMS viscosity in our individual batches, the spin-coater itself, or simply the need to produce our own calibration curve in order to accurately deposit the polymer at our desired thickness. Therefore, while spin-coating seems a promising method to coat our thermal emitters, we have yet to find a procedure to do so effectively. Although less precise, our final wafers have PDMS deposited using the blade-coating method from our initial testing. Spin-coating is discussed further in Appendix A. Future work may explore developing calibration curves to spin-coat PDMS, as well as measurement techniques to accurately measure layer thickness.

4.4 Summary

This chapter presents the final results of our rooftop passive cooling experiments. We observe sub-ambient passive cooling in both our silicon and fused silica devices under direct sunlight, as well as overnight. Also in this chapter, we document the multiple experiments, and modifications to both our fabrication process and experimental set-up to achieving our final results. Of particular importance are modifications to the emissive PDMS layer in our devices, which appears to enhance cooling potential. We also run several calibration experiments to ensure that our observed cooling is not a result of, or misconstrued by, offsets in our temperature sensors. We thus realize one of our primary goals of designing thermal emitters that can achieve passive daytime radiative cooling. Future work (see next chapter) may be required to maximize this cooling potential.

5. CONCLUSION AND FUTURE DIRECTIONS

Cooling is an essential component of many economic sectors and physical processes. The importance of cooling structures exposed to solar heating is only likely to increase for the foreseeable future under any climate warming scenario. Passive radiative cooling could supplement, or eventually replace, standard cooling methods, which are often costly and harmful to the environment [6][9]. Although passive cooling was long thought to be effective only for nighttime cooling of surfaces, the last decade has seen a myriad of approaches focused on daytime passive radiative cooling, which has the important benefit of actively cooling structures while they may otherwise be heated up by solar absorption [4] [9].

Our experiments aim to achieve passive cooling using relatively low-cost materials and simple fabrication techniques, that build on past work from the literature. While this project has generally sought to test the the approaches similar to those employed in [7] and [12], it has additionally focused on laying the groundwork for future passive cooling research at Pomona College.

As the first research project focused explicitly on passive cooling at Pomona, this work has achieved four benchmark goals. First, we developed a process for fabricating two types of passive cooling devices using relatively low-cost materials. Second, we designed and constructed an outdoor testing system for our devices and experimental controls. Third, we conducted testing for both types of thermal emitter devices, achieving a maximum sub-ambient cooling of 3.5°C in the daytime and 3.7°C during the nighttime. Our silicon wafers, which realized a slightly smaller margin of sub-ambient daytime cooling of 3.2°C, additionally cooled to an average > 20 °C below the bare silicon control. Finally, we have begun to lay out a theoretical framework for passive cooling that will ideally inform future experimental research and modeling. In addition to the completed work detailed in this thesis, this chapter also highlights several areas of future work.

5.1 Future Directions

The demonstrated cooling in our experiments, both relative to ambient temperatures as well as controls, is a promising proof-of-concept that lays a solid foundation from which to build towards our long-term goals to achieve significant cooling ($>10^{\circ}\text{C}$) below ambient temperatures. This section outlines a number of modifications to the experimental set-up, fabrication process, and data analysis, that could improve cooling performance, as well as data collection.

5.1.1 Experimental Set-Up

5.1.1.1 *Collecting Temperature Data*

The results presented in this thesis are intended to serve as a proof-of-concept test, both evaluating the radiative effects of passive cooling, as well as developing the fabrication process and measurement methodologies. In the case of our outdoor experiments, one area that will benefit from improvement is the process for logging temperature data. It is noted in Chapter 4 that the TMP36 temperature probes that we use have a higher margin of uncertainty than is desired, from ± 1.0 to $\pm 2.0^{\circ}\text{C}$ depending on the temperature range. Although our measured uncertainty is conservatively taken to be only $\pm 1^{\circ}\text{C}$, future work may consider using a sensor with a higher precision, such as a thermistor or thermocouple, so long as the probe is able to accurately measure the temperature of the wafers with which it is in direct contact.

Related to the specifics of the temperature sensors is the temperature logging set-up itself. The TMP36 sensors are wired into a breadboard, which is connected to an Arduino Uno micro-processor. This set-up has the added convenience of switching out probes that may be faulty or rearranging wiring to account for changes in the wafers being tested. However, this also adds a risk of wire connections becoming loose or bent, an issue that arose frequently in our experimental set-up. Once reliable individual probes are identified and the device array is finalized, a simple fix to this problem would be to solder together the individual components to ensure wired connections are secure.

Another key component of the circuit is our data logger. Our data is recorded on an SD card

via a data logger shield that fits directly over the Arduino Uno unit. This is a straightforward way to take data using the Arduino software interface, but connecting the logger to the Arduino limits the number of temperature probes that can be tested simultaneously. Since we would like to test our silicon and silica wafers in the same conditions, it would be ideal to use a microprocessor and data logger that can take data for both sets of wafers and their controls in identical environmental conditions. Future work may therefore consider using a microprocessor with the capacity to take temperature data for more sensors simultaneously, such as the Arduino Mega.

Adaptations to the temperature-logging process are not strictly necessary, and the current set-up is capable of taking and recording the temperature observations for outdoor experiments. These changes could, however, reduce the margin of error for data recorded, reduce the risk of equipment failures, and improve the rigor of inter-experiment comparisons by allowing more devices to be tested simultaneously.

5.1.1.2 Wind Covers

Results from the literature often include "IR-transparent" wind covers in their experimental set-ups, which are intended to minimize the influence on temperature from convective losses due to airflow adjacent to the emitter. Some of our initial testing included a cover placed over the top of the wafer-housing dishes, just above the wafer itself. However, we realized that while transparency in the mid-infrared portion of the electromagnetic spectrum is ideal for cooling, the variability in spectral absorption across the electromagnetic spectrum in the wind covers themselves makes it difficult to disentangle the radiative characteristics in the wind covers from the emitters. In other words, by using such a wind cover that has its own spectral properties, we cannot determine how much cooling, or lack thereof, can be attributed to the materials used in our thermal emitter versus the wind cover. This is especially true if the wind cover reflects sunlight. For these reasons, the final results in this thesis come from experiments that *do not* use a cover. Future work should make use of a wind cover, as parasitic heat gain from air flow is both likely and undesirable. The spectral properties of any cover used, however, should be analyzed to determine the potential impact on cooling performance. This can even be done via direct measurement, described in the next section.

5.1.2 Spectral Analysis

Radiative cooling is based on combining materials with specific spectral characteristics. In particular, we are interested in material combinations that are highly *reflective* over solar wavelengths and highly *emissive* over mid-infrared wavelengths. This thesis cites past literature on passive cooling, as well as documented reflectance and emittance standard measurements for the materials employed in our emitters to support our experimental design. Moving forward, however, it will be important to verify experimentally the spectral properties of the *entire* emitter, as opposed to relying on information for individual material layers. This is important for two reasons: (1) reflectance and emittance data for individual materials layered within the thermal emitter do not account for discrepancies in energy transfer or scattering at the layer interface; and (2) literature results for spectral properties in the materials we use do not account for physical variability in our specific devices, such as surface thickness and uniformity. Direct measurement is therefore highly desirable.

A number of approaches exist to obtain these measurements. For example, the Newport IQE-200b machine in the Pomona solar cell characterization instrument suite can be used to measure total reflectance of a sample over wavelengths ranging from 350 nm - 1100 nm, which would sufficiently cover the solar spectrum region in which we are interested. Assuming transmittance to be zero, we can solve for absorptance by using subtracting reflectance as $\alpha = 1 - R$. Obtaining similar measurements in the mid-infrared region is a bit more challenging, although the use of Fourier Transform Infrared Spectroscopy (FTIR) can be used to obtain reflectance, absorptance and transmittance values across wide swaths of the infrared spectrum. FTIR attachments such as an integrating sphere could be extremely useful in carrying out these measurements for multiple sample types, including the multi-layered stacks used in this set of experiments.

5.1.3 Theory and Calculations

This work measures cooling by directly taking temperature data in our devices and controls. One area for future exploration would be to use the theoretical framework laid out in Chapter 2 to

explicitly calculate cooling power in our devices. These calculations may be aided by using device simulation packages such as those provided by Simulink to model our sample devices.

5.1.4 Novel Device Structures

One of the key findings from this work is that the thickness of the PDMS seems to be an important factor in cooling potential. Future work may consider calibrating cooling potential, varying both the thickness and uniformity of the emissive layer. Additionally, the testing apparatus can be used for different device types that could build on other results from the literature, such as using dielectric stacks or super-cool paints [6][4].

5.2 Concluding Remarks

As global demand for cooling increases, electricity-free passive cooling may become integral to preventing overheating in buildings, electronic devices and other materials. As a relatively new, yet rapidly-expanding area of research, passive daytime radiative cooling has been attempted via many approaches, which span a wide range of material costs and required engineering. This project contributes to the field by testing a proof-of-concept passive cooling apparatus to compare multiple demonstrated approaches in the same environment with a consistent fabrication process. We focus on using relatively low-cost materials with a small upfront cost and short fabrication time, traits that are highly desirable for any future commercial development of passive cooling technologies. While we do not observe levels of cooling that approach significant theoretical limits [4], we do observe cooling to temperatures below ambient surrounding air, which is a key trait of passive cooling.

We also observe substantial cooling relative to our experimental controls. Based on these results and planned continued testing, our device approach could be extended to implementing passive cooling in building and rooftop materials which could, in turn, substantially reduce residential electricity consumption for air conditioning. In addition to building and testing passive cooling devices, this project also serves as a launchpad for future research into passive cooling at Pomona College. The author hopes that the fabrication process, testing apparatus, experimental approach,

and initial theoretical framework outlined in this thesis will support future work to expand upon the current project and contribute to this field of research.

REFERENCES

- ¹Y. Dong, M. Coleman, and S. A. Miller, “Greenhouse gas emissions from air conditioning and refrigeration service expansion in developing countries”, *Annual Review of Environment and Resources* **46**, 59–83 (2021).
- ²E. A. Goldstein, A. P. Raman, and S. Fan, “Sub-ambient non-evaporative fluid cooling with the sky”, *Nature Energy* **2**, 1–7 (2017).
- ³M. Isaac and D. P. van Vuuren, “Modeling global residential sector energy demand for heating and air conditioning in the context of climate change”, *Energy Policy* **37**, 507–521 (2009).
- ⁴Y. Yang and Y. Zhang, “Passive daytime radiative cooling: principle, application, and economic analysis”, *MRS Energy & Sustainability* **7**, Publisher: Cambridge University Press, 10 . 1557 /mre.2020.18 (2020).
- ⁵A. P. Raman, *Radiative cooling: optics enables access to the cold of space for energy on earth*, Feb. 16, 2021.
- ⁶A. P. Raman, M. A. Anoma, L. Zhu, E. Rephaeli, and S. Fan, “Passive radiative cooling below ambient air temperature under direct sunlight”, *Nature* **515**, 540–544 (2014).
- ⁷L. Zhou, H. Song, J. Liang, M. Singer, M. Zhou, E. Stegenburgs, N. Zhang, C. Xu, T. Ng, Z. Yu, B. Ooi, and Q. Gan, “A polydimethylsiloxane-coated metal structure for all-day radiative cooling”, *Nature Sustainability* **2**, 718–724 (2019).
- ⁸T. Li, Y. Zhai, S. He, W. Gan, Z. Wei, M. Heidarinejad, D. Dalgo, R. Mi, X. Zhao, J. Song, J. Dai, C. Chen, A. Aili, A. Vellore, A. Martini, R. Yang, J. Srebric, X. Yin, and L. Hu, “A radiative cooling structural material”, *Science* **364**, Publisher: American Association for the Advancement of Science, 760–763 (2019).

⁹X. Sun, Y. Sun, Z. Zhou, M. A. Alam, and P. Bermel, “Radiative sky cooling: fundamental physics, materials, structures, and applications”, *Nanophotonics* **6**, Publisher: De Gruyter, 997–1015 (2017).

¹⁰C. G. Granqvist and A. Hjortsberg, “Radiative cooling to low temperatures: general considerations and application to selectively emitting SiO films”, *Journal of Applied Physics* **52**, 4205–4220 (1981).

¹¹H. Zhong, P. Zhang, Y. Li, X. Yang, Y. Zhao, and Z. Wang, “Highly solar-reflective structures for daytime radiative cooling under high humidity”, *ACS Applied Materials & Interfaces* **12**, 51409–51417 (2020).

¹²J.-l. Kou, Z. Jurado, Z. Chen, S. Fan, and A. J. Minnich, “Daytime radiative cooling using near-black infrared emitters”, *ACS Photonics* **4**, Publisher: American Chemical Society, 626–630 (2017).

¹³J. Mandal, Y. Fu, A. C. Overvig, M. Jia, K. Sun, N. N. Shi, H. Zhou, X. Xiao, N. Yu, and Y. Yang, “Hierarchically porous polymer coatings for highly efficient passive daytime radiative cooling”, *Science* **362**, 315–319 (2018).

¹⁴W. Li and S. Fan, “Radiative cooling: harvesting the coldness of the universe”, *Optics and Photonics News* **30**, 32 (2019).

¹⁵A. R. Gentle and G. B. Smith, “A subambient open roof surface under the mid-summer sun”, *Advanced Science* **2**, 1500119 (2015).

¹⁶C. S. B. Grimmond and T. R. Oke, “Turbulent heat fluxes in urban areas: observations and a local-scale urban meteorological parameterization scheme (LUMPS)”, *Journal of Applied Meteorology and Climatology* **41**, Publisher: American Meteorological Society Section: Journal of Applied Meteorology and Climatology, 792–810 (2002).

¹⁷G. Perrakis, A. C. Tasolamprou, G. Kenanakis, E. N. Economou, S. Tzortzakis, and M. Kafesaki, “Combined nano and micro structuring for enhanced radiative cooling and efficiency of pho-

tovoltaic cells”, Scientific Reports **11**, Number: 1 Publisher: Nature Publishing Group, 11552 (2021).

¹⁸A. P. Raman, W. Li, and S. Fan, “Generating light from darkness”, Joule **3**, 2679–2686 (2019).

¹⁹J. P. Bijarniya, J. Sarkar, and P. Maiti, “Review on passive daytime radiative cooling: fundamentals, recent researches, challenges and opportunities”, Renewable and Sustainable Energy Reviews **133**, 110263 (2020).

²⁰C. Meola, S. Boccardi, and G. m. Carlomagno, “Chapter 3 - infrared thermography basics”, in *Infrared thermography in the evaluation of aerospace composite materials*, edited by C. Meola, S. Boccardi, and G. m. Carlomagno (Woodhead Publishing, Jan. 1, 2017), pp. 57–83.

²¹O. Stenzel, “Planar interfaces”, in *The physics of thin film optical spectra: an introduction*, edited by O. Stenzel, Springer Series in Surface Sciences (Springer International Publishing, Cham, 2016), pp. 97–129.

²²M. Brunetti and F. Prodi, “The climate system”, EPJ Web of Conferences **98**, 02001 (2015).

²³A. Srinivasan, B. Czapla, J. Mayo, and A. Narayanaswamy, “Infrared dielectric function of polydimethylsiloxane and selective emission behavior”, Applied Physics Letters **109**, Publisher: American Institute of Physics, 061905 (2016).

²⁴*Top 10 thermally conductive materials*, Thermtest Inc. <https://thermtest.com/thermal-resources/top-10-resources/top-10-thermally-conductive-materials>.

²⁵*Polydimethylsiloxane*, American Chemical Society, <https://www.acs.org/content/acs/en/molecule-of-the-week/archive/p/polydimethylsiloxane.html>.

²⁶S. Cargou, “PDMS membrane: thickness of a spin coated PDMS layer”, Elveflow, Publisher: Elvesys (2020).

APPENDIX A

DEVICE FABRICATION PROCESS

The final fabrication method for our passive radiative cooling devices is described in Chapter 3, with additional detail provided in Chapter 4 documenting the progression from our initial prototypes to our final device design. This appendix is intended to provide additional details about the device preparation and development process, as well as to mention a few areas for improvement that we were not able to use in our device design.

A.1 Wafer Preparation and Cleaning

Since our silicon and fused silica wafers were new and contained in dust-free containers, our cleaning process for wafers prior to deposition of silver and PDMS is minimal. We determined that a single round of plasma cleaning for each wafer would suffice to ensure clean layer deposition. Always be sure to use gloves and preferably tweezers when handling the wafers to avoid smudges, and minimize direct exposure to air and dust. Wafers should be stored either in the original rack from the manufacturer or petri dishes.

Notes on using the plasma cleaner

The plasma cleaner is kept in the Pomona College Chem Prep lab, with a short set of instructions that make the process user-friendly. The wafer can be kept in a petri dish which can be set directly in the plasma cleaner. Running the pump reduces the pressure inside the chamber prior to initiating the plasma. In order for this to work, you must *manually press the door closed* until you see the pressure start to drop on the meter atop the device. Once the door is sealed, you can follow the directions in the manual to initiate the plasma. The instructions are set up so that you can move on to the next step after certain pressure has been reached. Since the pressure fluctuations are rather high, you can progress through the steps within ± 10 mTorr.

A.2 Using the Thermal Evaporator

A.2.1 General Notes

Using the thermal evaporator to deposit reflective silver onto the substrates is a time-consuming process, but the manual in the chem prep lab is very useful. Since the evaporator is kept near vacuum pressure, much of the time during use is to allow the evaporator to "vent" to atmospheric pressure so that the substrates can be put into the device, and then "pumping the evaporator down" so that the silver can be deposited under near-vacuum. The evaporator must be vented again to remove the substrate. The details for each of these steps is listed in the device manual, but approximately 60 to 80 minutes should be allotted for the deposition. Additionally, because of the size of our wafers, only one wafer can fit on the deposition plate at a time. Doing multiple depositions one after the other saves time by allowing you to swap out your silver-coated wafer with a bare substrate when opening the chamber door rather than having to pump down the evaporator after each deposition.

A.2.2 Specific for PDRC Silver Deposition

The deposition plate is removable, allowing you to attach your substrate to the plate outside of the evaporator. The wafer must be adhered to the deposition plate since it is turned upside down in the evaporator to complete the deposition. Use four sets of screws and clips to secure the substrate, making sure not to screw the clips in too tight or else the wafer will crack. Do not use double-sided tape for this process, as it can lead to the wafer cracking when you try to remove it following the deposition. When putting your substrate in the evaporator, be sure to load four silver pellets into the silver deposition bed. This is necessary to layer silver at the current thickness of 120 nm. After putting your substrate in the evaporator, you can navigate to the "Main" menu and click "Load Recipe." The recipe for the PDRC device at the time of writing is in the "Hudgings" folder, titled "passiveCool-SRC4-Ag-smallAluminaBoat.rcp". You can check to make sure the recipe is loaded by navigating to "Recipe" -> "Deposit" -> "Deposit Rate" and make sure the display shows 1200 Å (120 nm) of silver (Ag).

A.3 Application of Polydimethylsiloxane

A.3.1 Mixing PDMS

Polydimethylsiloxane (PDMS) comprises the emissive layer in our radiative cooling devices. There are two methods we have used to mix PDMS, both of which involve mixing an elastomer base and a curing agent in a 10:1 ratio or base:curing agent. The specific product for the PDMS mixing kit is Sylgard 184, which we have purchased from Sigma Aldrich.¹ Sylgard 184 can be purchased in discrete 10 g "clip packs" which allow the PDMS to be mixed in the preset 10:1 ratios, or as bulk orders of base and curing agent. Both of these methods will produce PDMS that can be layered onto the PDRC devices. If you use the the base and curing agent in bulk, the ratios can be measured out manually with separate syringes in a plastic dish and mixed together with a glass stirring rod. We find that 10 mL of base with 1 mL of curing agent is sufficient to coat two to three wafers easily depending on the thickness. Mix the PDMS continuously for five minutes, and then let sit covered in the fume hood for three hours or until all bubbles have dissipated.

A.3.2 Blade Coating Procedure

Blade coating, also known as "doctor blading" is a method to deposit liquid thin films onto a substrate.² Since we want a specific PDMS thickness in our devices, we place a template over the silver-coated wafer, which is made out of compressed paper at a set thickness of $500 \mu\text{m} \pm 50 \mu\text{m}$. We laser cut a circle into the paper with a diameter of 98 mm. This is slightly smaller than the 100 mm diameter wafers, meaning that the paper edge of the template sits just inside the perimeter of the wafer. Pour PDMS onto the edge of the substrate in excess, ensuring that it stays inside the perimeter of the template. To make sure the paper templates can be reused, we also laser cut several identical holes into wax paper sheets that can be laid over the template to protect from any excess PDMS sticking to the paper.

Next, use a Teflon spatula to sweep the PDMS across the substrate, ensuring the spatula main-

¹For more information on PDMS specifications: <https://www.sigmaaldrich.com/US/en/product/aldrich/761036>

²More information on blade coating: <https://www.ossila.com/pages/solution-processing-techniques-comparisonDoctorBlading>

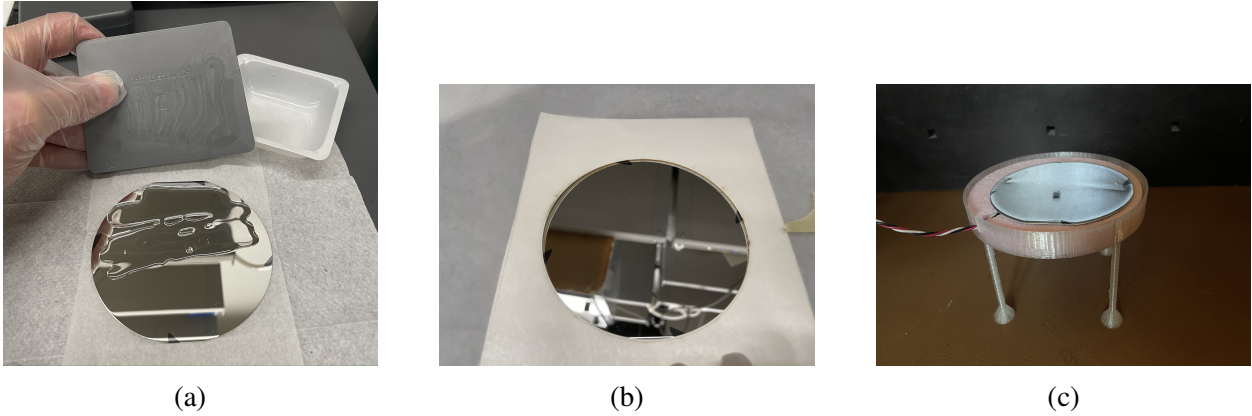


Figure A.1: (a) PDMS poured onto a silver-coated silicon wafer without the blade coating template applied, and Teflon spatula used for blade coating procedure; (b) Compressed paper template laid over a silver-coated silicon wafer prior to PDMS deposition; (c) Silicon PDRC device with PDMS layer after curing.

tains contact with the template edges. It is ideal to coat as much of the wafer as possible with one sweep from the spatula, although it is possible that additional sweeps may be needed to coat the entire wafer.

Once the substrate has been coated, it can be set on a hot plate at 100 °C for 45 minutes to cure. PDMS will cure at room temperature over time, but rapid curing ensures that the coating solidifies more uniformly. The coated wafer can now be stored in a petri dish or set in a PDRC stand for outdoor testing. Thickness of PDMS can be calculated by measuring the thickness of the entire coated wafer with an EZ Cal Caliper (uncertainty of 0.1 mm (100 µm)) and subtracting the thickness of the wafer substrate and silver layer.

A.3.3 Spin-Coating Method

Although we use the blade coating method in our final devices to coat PDMS, future work should consider using a spin coating method, which could be more precise and allow for a more uniform coating. In this project, we have conducted preliminary investigations into using the spin-coating procedure, but found that the PDMS thickness was consistently lower than desired. Some prior research has been done to calibrate PDMS thickness as a function of spin time and RPM (see Figure A.2) that can serve as a reference; however, an additional calibration may be needed for

thicknesses at or above 100 μm [26].

More information on spin-coating generally and spin-coating PDMS can be accessed at the following sites:

- **Spin-coating description:** <https://www.ossila.com/pages/solution-processing-techniques-comparison#DipCoating>
- **Spin-coating: PDMS:** <https://www.elveflow.com/microfluidic-review/s/soft-lithography-microfabrication/pdms-membrane-thickness-of-a-spin-coated-pdms-layer/>

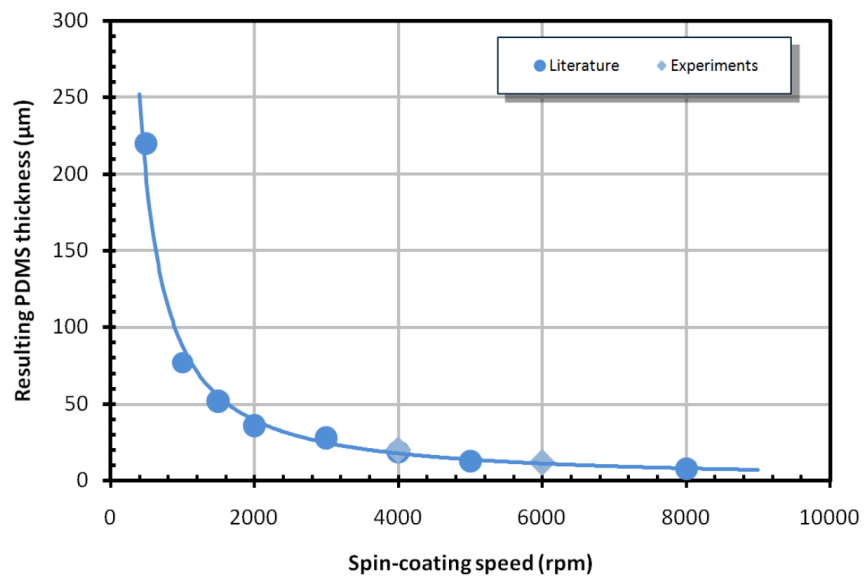


Figure A.2: PDMS spin-coating calibration curve. For thicknesses >100 μm , the ideal RPM value becomes uncertain.

APPENDIX B

TEMPERATURE LOGGING TESTING APPARATUS

B.1 General Notes on Experimental Set-Up

The experimental testing apparatus is described in Chapter 3, with additional comments in Chapter 4, section 3 detailing adaptations. The code for the Arduino data-logger is attached below, with comments about each code component. The code itself combines several pre-written scripts from Adafruit and SparkFun. Additional specifications for the temperature sensors and data logger can be accessed at the following pages:

- **TMP36 Sensors:** <https://learn.adafruit.com/tmp36-temperature-sensor/using-a-temp-sensor>
- **Adafruit Datalogger Shield:** <https://learn.adafruit.com/adafruit-data-logger-shield>

The TMP36 sensors must be soldered to three wires each, one which goes to ground, one to the 5V Arduino pin, and one to the analog pin. Analog pin assignments can be changed, but are set in our experiments are as follows:

- Pin 0: Ambient
- Pin 1: PDRC Device
- Pin 2: Silver Control
- Pin 3: Bare Wafer Control

B.2 Arduino Code

The code for the Arduino data logger combines several pre-set scripts from Adafruit and Sparkfun to use the Adafruit data logger and to use TMP36 sensors. Note that we use a HiLetgo data

logger, which has the same functionality and design as the Adafruit model. The code used in our experiments is attached below, and the original preset scripts can be accessed at the following links.

- **Adafruit Data Logger:** <https://learn.adafruit.com/adafruit-data-logger-shield/using-the-real-time-clock-3>
- **TMP36 Code:** <https://learn.adafruit.com/tmp36-temperature-sensor/using-a-temp-sensor>

```
#include <Adafruit_I2CDevice.h>
#include <Adafruit_I2CRegister.h>
#include <Adafruit_SPIDevice.h>
#include <Adafruit_BusIO_Register.h>
#include <SPI.h>
#include <SD.h>
#include <Wire.h>
#include "RTCLib.h"
```

```
/*
```

DISCLAIMER: This code, including much of the commenting is adapted from two scripts written by SparkFun; one to record temperature data using TMP36 sensors, and another to write data to an SD card using an Arduino shield attachment.

From Sparkfun:

"When looking at the flat side of the temperature sensor with the pins down, from left to right the pins are:
5V, SIGNAL, and GND.

Connect the 5V pin to 5 Volts (5V).
Connect the SIGNAL pin to ANALOG pin 0.
Connect the GND pin to ground (GND).

This code is completely free for any use.
Visit <http://learn.sparkfun.com/products/2> for SIK information.
Visit <http://www.arduino.cc> to learn about the Arduino.

Version 2.0 6/2012 MDG"

```
*/
```

```
// Including definitions for data logger
```

```
// how many milliseconds between grabbing data and logging it. 1000 ms is once a second
#define LOG_INTERVAL 1000 // mills between entries (reduce to take more/faster data)
```

```
// how many milliseconds before writing the logged data permanently to disk
// set it to the LOG_INTERVAL to write each time (safest)
// set it to 10*LOG_INTERVAL to write all data every 10 datareads, you could lose up to
// the last 10 reads if power is lost but it uses less power and is much faster!
#define SYNC_INTERVAL 60000 // mills between calls to flush() - to write data to the card
uint32_t syncTime = 0; // time of last sync()
```

```
#define ECHO_TO_SERIAL 1 // echo data to serial port
#define WAIT_TO_START 0 // Wait for serial input in setup()
```

```
// the digital pins that connect to the LEDs
#define redLEDpin 2
#define greenLEDpin 3
```

```
// We'll use analog inputs 0-4 to measure the temperature sensor's
// signal pin.
//this sets for 4 temperatures sensors, one of which measures ambient

const int ambientPin = 0;
const int waferPin1 = 1;
const int waferPin2 = 2;
const int waferPin3 = 3;

//define a function to read the voltage measured at the analog pins
//this voltage can then be used to compute temperatures in the TMP36 sensors

float getVoltage(int pin)
{
    //this determines the voltage for a reference voltage of 5V
    return (analogRead(pin) * 0.00488281);

}

//Now set up the components of the data logger

//start with the built-in clock
RTC_PCF8523 RTC; // define the Real Time Clock object
//(this may need to be changed depending on which data logger model used)

// for the data logging shield, we use digital pin 10 for the SD cs line
const int chipSelect = 10;

// the logging file
File logfile;

void error(char *str)
{
    Serial.print("error: ");
    Serial.println(str);

    // red LED indicates error
    digitalWrite(redLEDpin, HIGH);

    while(1);
}

void setup(void)
{
    Serial.begin(9600);
    Serial.println();
```

```

// use debugging LEDs
pinMode(redLEDpin, OUTPUT);
pinMode(greenLEDpin, OUTPUT);

#if WAIT_TO_START
  Serial.println("Type any character to start");
  while (!Serial.available());
#endif //WAIT_TO_START

//SET UP THE SD CARD AND DATA LOGGER TO RECORD YOUR DATA

// initialize the SD card
Serial.print("Initializing SD card...");
// make sure that the default chip select pin is set to
// output, even if you don't use it:
pinMode(10, OUTPUT);

// see if the card is present and can be initialized:
if (!SD.begin(chipSelect)) {
  error("Card failed, or not present");
}
Serial.println("card initialized.");

// create a new file
//COMMENT OUT FOR TRIAL TESTING WITHOUT LOGGING TO A NEW FILE
char filename[] = "LOGGER00.CSV";
for (uint8_t i = 0; i < 100; i++) {
  filename[6] = i/10 + '0';
  filename[7] = i%10 + '0';
  if (! SD.exists(filename)) {
    // only open a new file if it doesn't exist
    logfile = SD.open(filename, FILE_WRITE);
    break; // leave the loop!
  }
}

if (! logfile) {
  error("couldnt create file");
}

Serial.print("Logging to: ");
Serial.println(filename); //END COMMENT HERE

// connect to RTC
Wire.begin();
if (!RTC.begin()) {
  logfile.println("RTC failed");
#if ECHO_TO_SERIAL
  Serial.println("RTC failed");
#endif //ECHO_TO_SERIAL

```

```

}

  logfile.println("millis,stamp,datetime,ambTemp,temp1,temp2,temp3");
#if ECHO_TO_SERIAL
  Serial.println("millis,stamp,datetime,ambTemp,temp1,temp2,temp3");
#endif //ECHO_TO_SERIAL

}

void loop(void)
{
  //log the date and time stamp

  //uncomment this line if the real time clock needs to be reset
  //RTC.adjust(DateTime(F(__DATE__), F(__TIME__)));
  //DateTime now;

  // delay for the amount of time we want between readings
  delay((LOG_INTERVAL -1) - (millis() % LOG_INTERVAL));

  digitalWrite(greenLEDpin, HIGH);

  // log seconds since starting
  uint32_t m = millis();
  logfile.print(m/1000);           // milliseconds since start
  logfile.print(", ");
#if ECHO_TO_SERIAL
  Serial.print(m/1000);           // milliseconds since start
  Serial.print(", ");
#endif

/*NOTE: As of 05/01/2022 the RTC process below does not work.
it is left in the script for now because it does not prevent data collection
and would be ideal to have. It currently warrants debugging or hardware adaptations*/
  // fetch the time
DateTime now = RTC.now();
  // log time
  //logfile.print(now.unixtime()); // seconds since 1/1/1970
  logfile.print(", ");
  logfile.print('\'');
  logfile.print(now.year(), DEC);
  logfile.print("/");
  logfile.print(now.month(), DEC);
  logfile.print("/");
  logfile.print(now.day(), DEC);
  logfile.print(" ");
  logfile.print(now.hour(), DEC);
  logfile.print(":");
  logfile.print(now.minute(), DEC);
}

```

```
logfile.print(":");
logfile.print(now.second(), DEC);
logfile.print('');

//write the same thing to the serial monitor
#if ECHO_TO_SERIAL
    //Serial.print(now.unixtime()); // seconds since 1/1/1970
    Serial.print(", ");
    Serial.print('\'');
    Serial.print(now.year(), DEC);
    Serial.print("/");
    Serial.print(now.month(), DEC);
    Serial.print("/");
    Serial.print(now.day(), DEC);
    Serial.print(" ");
    Serial.print(now.hour(), DEC);
    Serial.print(":");
    Serial.print(now.minute(), DEC);
    Serial.print(":");
    Serial.print(now.second(), DEC);
    Serial.print('\'');
#endif //ECHO_TO_SERIAL
```

```
//NOW COLLECT TEMPERATURE DATA FROM ANALOG PINS
```

```
//declare float variables for the voltage and temperatures
float voltAmb, ambDegC, ambDegF;
float voltWaf1, waf1DegC, waf1DegF;
float voltWaf2, waf2DegC, waf2DegF;
float voltWaf3, waf3DegC, waf3DegF;

//voltage and temperatures for the ambient pin currently connected to the breadboard
voltAmb = getVoltage(ambientPin);
ambDegC = (voltAmb - 0.5) * 100.0;
ambDegF = ambDegC * (9.0/5.0) + 32.0;
delay(100);

//compute the voltage and temperatures for the first wafer pin
voltWaf1 = getVoltage(waferPin1);
waf1DegC = (voltWaf1 - 0.5) * 100.0;
waf1DegF = waf1DegC * (9.0/5.0) + 32.0;
delay(100);

//compute the voltage and temperatures for the second wafer pin
voltWaf2 = getVoltage(waferPin2);
waf2DegC = (voltWaf2 - 0.5) * 100.0;
waf2DegF = waf2DegC * (9.0/5.0) + 32.0;
delay(100);

//compute the voltage and temperatures for the 3rd wafer pin
```

```

voltWaf3 = getVoltage(waferPin3);
waf3DegC = (voltWaf3 - 0.5) * 100.0;
waf3DegF = waf3DegC * (9.0/5.0) + 32.0;

//Log the data
logfile.print(",");
logfile.print(ambDegC);
logfile.print(",");
logfile.print(waf1DegC);
logfile.print(",");
logfile.print(waf2DegC);
logfile.print(",");
logfile.print(waf3DegC);

#if ECHO_TO_SERIAL
Serial.print(",");
Serial.print(ambDegC);
Serial.print(",");
Serial.print(waf1DegC);
Serial.print(",");
Serial.print(waf2DegC);
Serial.print(",");
Serial.print(waf3DegC);
#endif //ECHO_TO_SERIAL

logfile.println();
#if ECHO_TO_SERIAL
Serial.println();
#endif // ECHO_TO_SERIAL

digitalWrite(greenLEDpin, LOW);

// Now we write data to disk! Don't sync too often - requires 2048 bytes of I/O to SD card
// which uses a bunch of power and takes time
if ((millis() - syncTime) < SYNC_INTERVAL) return;
syncTime = millis();

// blink LED to show we are syncing data to the card & updating FAT!
digitalWrite(redLEDpin, HIGH);
logfile.flush();
digitalWrite(redLEDpin, LOW);

}

```